

# Vivaldi Antenna Array for a Solid-State Space Distributed Amplifier

by

Alix Rivera-Albino

A thesis submitted in partial fulfillment of the requirements for the degree of

MASTER OF SCIENCE  
in  
ELECTRICAL ENGINEERING

UNIVERSITY OF PUERTO RICO  
MAYAGÜEZ CAMPUS  
2009

Approved by:

---

José Colom-Ustariz, PhD  
Member, Graduate Committee

---

Date

---

Nelson Sepúlveda-Alancatro, PhD  
Member, Graduate Committee

---

Date

---

Rafael Rodríguez -Solís, PhD  
President, Graduate Committee

---

Date

---

Darrell Hajek, PhD  
Representative of Graduate Studies

---

Date

---

Isidoro Couvertier-Reyes, PhD  
Chairperson of the Department

---

Date

## ABSTRACT

This work reports the design of a Vivaldi antenna array for a space distributed solid state amplifier at X-Band and the specifications in the amplifier design. A tray configuration inside an over-moded waveguide is used. The waveguide operates in its  $TE_{30}$  mode, which allows for 3, 6 or 9 trays to be positioned for increasing power generation. Each tray has four class-E amplifiers, and the input and output devices to each of the amplifiers are Vivaldi antennas. This work shows the tapered-slot antennas design for the desired impedance based on their tray position. The two center antennas and the two edge antennas on each tray are kept with same dimensions to simplify the Design of Experiments analysis. It was found that although the center frequency of operation is shifted up 3MHz when comparing 3, 6 and 9 trays configurations, the antenna behavior does not change significantly. Thus, the same antenna design can be used for all trays. The antennas were simulated, built and tested for an input impedance of  $65 \Omega$ , and simulated for  $24 \Omega$  and  $50 \Omega$ . Because of the difficulty to build low impedance antennas, only antennas of  $50 \Omega$  were used. This required matching networks to provide the required transistor impedance to act as a class- E module. A stub at the second harmonic is added to the  $50 \Omega$  design in order to decrease the power consumption of the transistor. The class-E module design and the setup to test it are reported. Finally, the complete tray to implement the spatially distributed amplifier is shown.

## RESUMEN

Este trabajo muestra el diseño de un arreglo de antenas tipo Vivaldi para un amplificador banda-X de estado sólido distribuido en espacio. Se utiliza una guía de onda operando en el modo  $TE_{30}$ , el cual permite que se coloquen 3, 6 ó 9 tarjetas de manera que se aumente la generación de potencia. Cada tarjeta tiene cuatro amplificadores clase-E, cuyas entradas y salidas son antenas Vivaldi. Se muestra el diseño de las antenas para la impedancia deseada basado en la posición de éstas en la tarjeta. Las antenas del centro y las antenas de las esquinas se mantienen con las mismas dimensiones para simplificar el análisis del diseño de experimento que se usa para caracterizar las antenas. De éste se encuentra, que según se aumenta el número de tarjetas el ancho de banda disminuye sólo 3 MHz y la frecuencia de operación se mueve hacia arriba menos de 3MHz. Las antenas son simuladas, construidas y medidas para  $65 \Omega$ , lo que sirve de base para diseñar las de  $24 \Omega$  y  $50 \Omega$ . Sin embargo, dada la dificultad para construir antenas de baja impedancia, se deciden usar antenas de  $50 \Omega$  en la entrada y en la salida. Dado esto se tienen que utilizar redes de pareo para proveer al transistor la impedancia de salida necesaria para actuar como clase-E. A este diseño se le añade una terminación para eliminar la segunda armónica y de esta manera reducir el consumo de potencia. El diseño del amplificador clase-E y el montaje necesario para hacer sus medidas es mostrado. Finalmente, se muestra el diseño de una tarjeta completa para ser utilizada en el amplificador distribuido en espacio.

**FOR THOSE WHO HAVE THE COURAGE TO FIGHT FOR HAPPINESS  
AND  
TO THE PERSON WHO GIVES ME THE SUPPORT TO DO IT.**

## ACKNOWLEDGEMENTS

First, I want to thank God for giving me the privilege to enjoy this beautiful stage of my life and the courage to overcome it. Second, to my husband Edgar Martí for his support and never allowing me to give up.

Especially, I want to thank my mom (Bruny) because she was my inspiration to this success. Thanks to my dad (Luis), my brothers (Luis, Alejandro, Alfonso and Armando) and my sisters (Awilda, Marisol, and Luisa) for believing in me. I love you!

Thanks to my Professor Rafael Rodríguez Solís for being my advisor and guiding me through this journey. Thanks for your counseling and corrections. Thanks to Professor Nelson Sepúlveda for being part of my committee and his help during this process. I greatly appreciate the help of Professor José Colom during these years.

I want to express my gratitude to the computer system administrator, Pablo Rebollo, for providing the computing resources to complete the simulation process. Thanks to Armando Rúa for helping me with the wire bonding process and to Professor Félix Fernández for letting me use his lab equipment. I appreciate the help of Néstor López for teaching me the basic steps to finish this project. I want to thank Jose Abdiel (Venture) for helping me in the wet etching process.

For those that listened to me every day and gave me their support: Carlitos and Ricky thanks for being there. Thanks to Jaime, Pablo (Biscui), Gianni, Navi, Kotshie, Febo, Alexandra, María Fernanda, Víctor, and Yilda because you were an important part of that stage.

Thanks to all, without you this could not be possible!

## TABLE OF CONTENTS

ABSTRACT .....	ii
RESUMEN .....	iii
ACKNOWLEDGEMENTS .....	v
LIST OF TABLES .....	viii
LIST OF FIGURES .....	ix
1.1    MOTIVATION .....	2
1.2    SUMMARY OF FOLLOWING CHAPTERS .....	4
2.1    POWER AMPLIFIERS .....	5
2.2    CLASS-E MODULES .....	8
2.3    TAPERED SLOT ANTENNAS .....	12
2.4    TSA IN POWER AMPLIFIER APPLICATIONS .....	13
2.5    WAVEGUIDES .....	14
CHAPTER 3 METHODOLOGY .....	16
CHAPTER 4 DESIGN PROCEDURE .....	19
4.1    WAVEGUIDE .....	19
4.1.1    FIRST DESIGN .....	19
4.1.2    SECOND DESIGN .....	21
4.2    TAPERED SLOT ANTENNAS .....	21
4.2.1    SUBSTRATE SELECTION .....	21
4.2.2    FEED TYPE .....	22
4.2.3    ANTENNA GEOMETRY .....	22
4.2.4    ANTENNA GEOMETRY- SECOND DESIGN .....	23
4.3    CLASS-E AMPLIFIER .....	24
4.4    MATCHING AND BIAS NETWORKS .....	27
4.4.1    MATCHING NETWORK .....	27
4.4.2    BIAS NETWORK .....	28
4.5    SPATIALLY DISTRIBUTED AMPLIFIER .....	29
CHAPTER 5 RESULTS .....	30
5.1    WAVEGUIDE .....	30
5.1.1    WAVEGUIDE- FIRST DESIGN .....	30
5.1.2    WAVEGUIDE- SECOND DESIGN .....	31
5.2    ANTENNAS .....	33
5.2.1    DESIGN OF EXPERIMENT (DOE) .....	33

5.2.2	BEST PERFORMANCE WITH THREE TRAYS .....	35
5.2.3	MEASURED RESULTS.....	37
5.2.4	SIX AND NINE TRAYS.....	39
5.2.5	INPUT ANTENNAS- 50 $\Omega$ INPUT IMPEDANCE.....	41
5.2.6	OUTPUT ANTENNAS - 24 $\Omega$ INPUT IMPEDANCES .....	42
5.2.7	50 $\Omega$ ANTENNAS WITH STUB.....	43
5.3	OUTPUT MATCHING DESIGN .....	49
CHAPTER 6 CONCLUSION AND FUTURE WORK .....		51
6.1	CONCLUSION .....	51
6.2	CONTRIBUTIONS OF THIS WORK .....	51
6.3	FUTURE WORK.....	52
REFERENCES .....		53

## LIST OF TABLES

Table 4-1: Transversal electromagnetics modes for the 10 and 30 modes at 10GHz.....	20
Table 4-2: Transistors required impedance to operate as class-E and the maximum output power.....	24
Table 5-1: Dimensions for the 3, 6 and 9 trays for the 65 $\Omega$ Antennas, and the 3-Trays Simulations for the 50 $\Omega$ and 24 $\Omega$ Antennas. ....	47
Table 5-2: Matching network dimensions. ....	50

## LIST OF FIGURES

Figure 1-1: Proposed power amplifier design.....	2
Figure 2-1: 40W Broad-Band Spatial Power Combiner Configuration [2].....	6
Figure 2-2: Class-E circuit.....	9
Figure 2-3: Equivalent circuit for the class-E module [10] .....	10
Figure 2-4: Class-E Amplifier [11].....	11
Figure 2-5: Rectangular waveguide operating in TE <sub>10</sub> mode.....	14
Figure 3-1: Setup to test the class-E module .....	17
Figure 4-1: Configuration of the trays inside the over-mode waveguide..	19
Figure 4-2: Waveguide design.....	20
Figure 4-3: Second waveguide design .....	21
Figure 4-4: Tray configuration.....	23
Figure 4-5: The tray configuration.....	24
Figure 4-6: Transistor circuit.....	25
Figure 4-7: Setup to test the class-E module.....	25
Figure 4-8: Setup to test the amplifier.....	26
Figure 4-9: Matching network with an open stub.....	28
Figure 4-10: Bias Network.....	28
Figure 4-11: Complete tray design.....	29
Figure 5-1: S parameters for the overmoded waveguide.....	31
Figure 5-2: E-fields amplitude inside the waveguide.....	32
Figure 5-3: Setup to measure waveguide S parameters .....	32
Figure 5-4: S parameters for the second waveguide design .....	33
Figure 5-5: Significance of the effects of the design parameters in the edge antennas input impedance.....	34
Figure 5-6: Significance of the effects of the design parameters in the center antennas input impedance.....	35
Figure 5-7: Experiment with a four variable factorial design.....	36
Figure 5-8: Input resistance and reactance for the 65 $\Omega$ antennas .....	36
Figure 5-9: VSWR for the 65 $\Omega$ antennas.....	37

Figure 5-10: Design setup to measure antennas VSWR.....	38
Figure 5-11: VSWR for an edge antenna on an edge tray.....	38
Figure 5-12: Six trays configuration.....	39
Figure 5-13: VSWR for the six trays configuration.....	40
Figure 5-14: Nine trays configuration.....	40
Figure 5-15: VSWR for the nine trays configuration.....	41
Figure 5-16: Input resistance and reactance for the 50 $\Omega$ antennas.....	42
Figure 5-17: VSWR for the 50 $\Omega$ antennas.....	42
Figure 5-18: Input reactance for the 24 $\Omega$ antennas.....	43
Figure 5-19: VSWR for the 24 $\Omega$ antennas.....	43
Figure 5-20: Input resistance and reactance for the 50 $\Omega$ antennas with the stub.....	44
Figure 5-21: VSWR for the 50 $\Omega$ antennas with the stub.....	44
Figure 5-22: VSWR for the 50 $\Omega$ antennas at second harmonic.....	45
Figure 5-23: Simulated and measured results for two antennas in the three trays configuration.....	46
Figure 5-24: Setup to validate the 50 Ohms antenna design.....	47
Figure 5-25: VSWR for the 50 $\Omega$ antennas in the 9-tray configuration.....	48
Figure 5-26: Simulated and measured results for two antennas in the nine trays configuration.....	49
Figure 5-27: VSWR for the match network.....	50

# CHAPTER 1

## INTRODUCTION

High-power amplifiers are fundamental components in communications and radar systems. With these technology changes, the shift to higher frequency bands in these areas has caused a great impact. However, solid-state devices provide smaller amounts of power as the frequency increases. Consequently, it is often necessary to either use vacuum tubes or appropriately combine several solid-state devices to obtain the desired power output. Power combining can be divided into transmission line combining and spatial combining. Transmission line combining alternatives, such as corporate feeds, become more inefficient as the number of combined devices increases, because of increased losses due to longer transmission lines. In a parallel connection, as the number of devices increases, it is more difficult to provide an equal share of the biasing current to each device. Therefore, for a large number of devices, spatial combining becomes a viable alternative, even though the excitation amplitude and phase distribution may not be uniform across the active devices. The main advantage of spatial power combining is that it eliminates the need for complex and lossy feed lines. In addition, the losses remain constant as the number of devices increases [1]

This thesis presents the design of a Vivaldi antenna array to be used in a space-distributed power amplifier as an alternative for a X-band solid-state meteorological radar. The work follows the one presented in [1-5] but here the devices are operated in class-E mode to provide a higher efficiency. In addition, the waveguide housing the amplifier trays is designed to operate in the  $TE_{30}$  mode. That gives three maximum power regions in the guide, allowing the placing of more trays, and, thus, increasing the maximum power the amplifier can provide. The increased size of the waveguide also helps to improve the

thermal management in the amplifier. Figure 1-1 shows the proposed power amplifier design.

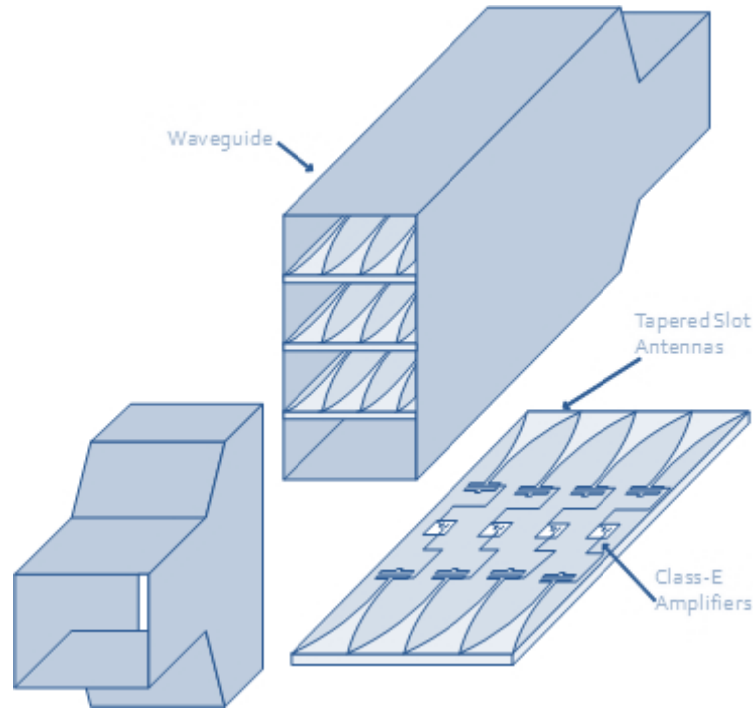


**Figure 1-1: Proposed power amplifier design.**

Tapered slot antennas (TSA) are used as the radiating elements. They are well suited for this application since they produce endfire radiation. The slots are fed through coplanar waveguide (CPW) since this makes possible to place of the amplifiers in the same plane of the antenna, and avoids the use of via-holes to connect the transistor source to ground.

## 1.1 MOTIVATION

One goal of CASA<sup>1</sup> is to implement a weather radar network in order to measure lower atmospheric phenomena in Puerto Rico. One part of that project is the development of X-band solid state Doppler radars with dual polarization. The main reasons to consider the use of solid-state radars are that they can be made coherent, allow the use of pulse

---

<sup>1</sup> Center for Collaborative Adaptive Sensing of the Atmosphere is a multi-sector partnership among academia, industry, and government dedicated to engineering revolutionary weather-sensing networks. These innovative networks will save lives and property by detecting the region of the lower atmosphere currently below conventional radar range - mapping storms, winds, rain, temperature, humidity, and the flow of airborne hazards. <http://www.casa.umass.edu/>

compression techniques, require less power than magnetron based radars, and do not need a high voltage modulator. In the Puerto Rico Testbed, the proposed radars will have a peak transmitted power in the order of 25-50 W. The two scanning alternatives considered for the radars are electronic scan in azimuth and mechanical scan in elevation, and mechanical scan in azimuth and elevation. The second configuration requires the use of a solid-state high-power amplifier instead of the current magnetron transmitter.

For this last configuration, two important characteristics for the selection of a power amplifier are the output power level and the efficiency. To increase the power level, it is necessary to combine the power of several devices. This combination can be performed spatially or with the use of transmission line splitters and combiners. However, research shows that when the power is combined spatially the losses are kept constant for a large number of elements. As a consequence, this configuration provides better efficiency compared to transmission line combiners.

Another important factor in the efficiency is the amplifier class of operation. Class A, B, AB and E have all been used to design power amplifiers. Efficiency and linearity play important roles in each class. Modules such as A, B and AB maintain a linear performance but their efficiency is relatively low (less than 50%). Class E have a great efficiency but has nonlinear performance. For a pulse-Doppler solid-state radar, efficiency is more important than linearity, since the pulse shape is not modulated and, for that reason, class-E modules are a viable alternative. The harmonic content produced by the amplifier non-linearities is reduced with the use of matching networks in the module design.

In general, research has been focused on high efficiency or high output power analysis. The goal of this thesis is to design a tapered slot antenna array to be used in a high power and high efficiency space-distributed amplifier using class-E modules. The tapered slot geometry simplifies the amplifier implementation.

## 1.2 SUMMARY OF FOLLOWING CHAPTERS

After this introduction, a more detailed description about this project is presented. Chapter 2 has the required background and literature review to understand this thesis. It includes a section of waveguides, a section of antennas and, finally, a section of power amplifier theory.

In Chapter 3, the methodology is presented. It consists of the basic steps to achieve the objectives of this thesis. It starts with the selection of transistors, characteristics of the antennas and waveguide transition. The setup for test the amplifier is shown. It ends with the implementation steps.

The design process of the work is presented in Chapter 4. It starts with a description of the waveguide design, followed by the antenna design procedure. In the antennas section, the design of 65 Ohms for three, six and nine trays are explained. Then, a second design for the antennas is presented, in which a second harmonic termination is added. The chapter continues with the selection of the transistor and ends with the design of the matching and bias networks.

The results are presented in Chapter 5. The first section is dedicated to show the results of the waveguide and a comparison with the simulated values. A design of experiment for 65 Ohms antennas is described showing its results. With it 6 and 9 trays are simulated and it gives the base to the design of 50 and 24 Ohms antennas. The results of the second harmonic termination are also shown. In this case a comparison between simulated and measured values is presented. Results from matching network simulations are showed. The chapter continues with description of the design of the class-E modules. Finally, a complete tray for the spatially distributed amplifier is shown.

The results are analyzed and the conclusions are presented in Chapter 6. Additionally, possible future work is mentioned in this chapter. As complementary resources, the references used through the thesis are at the end of this report.

# CHAPTER 2

## LITERATURE REVIEW

A crucial step in the design procedure is to know the basic concepts of each of the components of the amplifiers. This chapter is divided in four different sections: 1) the power amplifiers, 2) class-E modules, 3) tapered slot antennas, and 4) waveguides. In the power amplifiers section, different power amplifiers will be discussed together with their advantages and disadvantages. With respect to the class-E modules, the needed input and output impedances will be discussed, as well as the required matching circuits to obtain high efficiency. The design of the tapered slot antennas will be discussed. In that section, the input impedance and the antenna feed will be emphasized. Finally, a brief description of waveguides is discussed.

### 2.1 POWER AMPLIFIERS

Different power amplifiers have been analyzed separately by York and Popovic, and the reported output power is in the range of 40 W to 120 [1-7]. These amplifiers have been developed using class-A, class AB, or class-E modules with efficiencies lower than 70%.

In 1999, a 40W CW broad band spatial power combiner was reported [2]. In this case, Cheng, et. al. implemented the amplifier with 4 identical trays. Each tray consisted of two input tapered slot antennas, two MMIC power amplifiers and two output tapered slot antennas. This configuration is shown in Figure 2-1. One important point here is that the number of trays is limited by the waveguide aperture. Other important fact is that the trays in the center will receive more incident RF power than the others. Their results show that the center trays receive  $\frac{2}{3}$  of the incident power. In terms of output power, they obtained 41 W at 8.7 GHz and a bandwidth from 8 to 11 GHz.

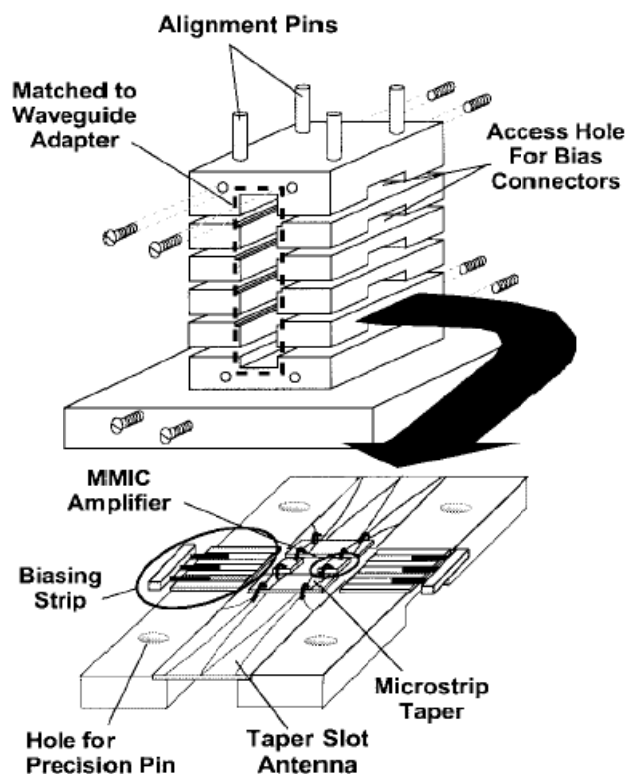


**Figure 2-1: 40W Broad-Band Spatial Power Combiner Configuration. Figure obtained from [2].**

Bryerton, et. al. compared spatial power combining with chip level combining in [6]. The goal in this article is to compare the efficiency in terms of the dc and RF powers. First, they designed a class-F and a class-E amplifier each with a different MESFET device. The class F amplifier had a MESFET physically larger than the MESFET of the class-E amplifier. They found that the MESFET with the larger physical area gives more output power, as expected, but the overall efficiency is lower. Then, they compared the spatial and circuit level combiner methods using the class-E and class-F amplifiers for each method. Their results show that the spatial combiner is more efficient with more amplifiers and in antennas applications since the EIRP (Effective isotropically radiated power) is higher and the thermal management is easier.

The principal advantage of the spatial power combiner is that when the number of elements is increased, the losses remain constant. In [3], another spatial power combiner

was designed. In this case, the output power was 60 W at 8 GHz. The design is similar to [2] but with 4 tapered slot antennas in each tray, and 4 trays in the system. Their results shows a 40% bandwidth with a return loss lower than -10dB. The maximum power was observed at 8 GHz and the PAE was 30%.

An extended work was presented in [4] where the output power increased to 120W. In this case, they used 6 trays, each with 4 MMIC, and 4 input and 4 output tapered slot antennas. As expected, the insertion and return losses deteriorated with more trays. Their results show a maximum of 126 W at 8.1GHz.

In 2000, an article about the advantages of the spatial power combined was published in the IEEE Microwave Magazine [1]. The authors showed a comparison between combining power by transmission lines or spatially. They showed that with the transmission line method the losses increase as the number of amplifiers increase and, therefore, the method become inefficient with larger number of amplifiers. In this article, a comparison between a tile and a tray array is also presented. The advantage of using a tray array is that it provides more isolation between the circuits and it facilitates the thermal management.

Pengcheng, et. al., focused in the design of finline arrays for spatial power combining in [5]. They presented the design process to provide the desired impedance to the MMIC in a determined bandwidth and used it to make different arrays systems. Their results show that with more antennas the coupling increases and the reflection losses are increased because they used the same antenna's impedance for the trays. A contribution of this thesis is to change the dimensions of the antennas in the tray to take in account the effects of the coupling.

In 2003, a spatial combiner was designed for X-band [7]. The first step was the class E modules design. They used the GaAS MESFET AFM04P2 and found the needed load impedance with a simple equation. The class-E modules design showed 60% drain efficiency and a 14 % frequency bandwidth at 10 GHz. The next step was to design the

antennas. The design consisted of two patches separated by air: one fed directly and one parasitic. The antennas results show a -27dB reflection coefficient, 11.6 % frequency bandwidth and a gain of 8.5dB. Once the class E modules and the antennas were designed, the power amplifier was built. They started with a design of four element array and the result had a gain of 13.5 dB. Then, a 16 element array was designed. In this case, the gain increased to 18.8 dB and 90% radiation efficiency at 10.2 GHz. The EIRP at 10.2 GHz was 162W.

## **2.2 CLASS-E MODULES**

Modules are an important part of power amplifiers since they establish the level of output power, linearity and efficiency. There are various classes of modules including A, B, C AB, D and E. Classifications of power amplifiers are based on two things: bias point dependence and switch types.

Classes A, B, C and AB are classified in bias point dependence. In class A, the transistor must operate in the entire RF cycle which gives less than 50 % efficiency. In this case, the performance of the amplifier is completely linear. If the transistor is forced to act only one half of the RF cycle, the module is class B. Class B modules have efficiency of 78%, but the increase of efficiency come at expense of loss of linearity. Class C modules operate in less than 50% of the RF cycle and achieve up to 87% efficiency but are highly nonlinear. Class AB module is a halfway between A and B in terms of linearity and achieves 67.9% of efficiency.

Some transistors can act like switches like classes E, D and F. In these cases the performance is completely non linear. However, in cases in where nonlinearity is not a significant issue, class-D and E are very attractive options. Especially, class E has become an interesting research theme recently since it is an excellent alternative for high efficiency requirements.

In [8], Cripps presents a theoretical description about class-E amplifiers. These amplifiers act like switches since they work in the saturation region, but as a consequence they are highly non-linear. In this class, the current is zero when the voltage has a maximum and vice versa. In this way, the power dissipation ( $P=IV$ ) will be zero and the efficiency will be 100%. Figure 2-2 shows the design presented by Cripps. One important parameter is  $C_p$  since it affects the RF output power as well as the efficiency.

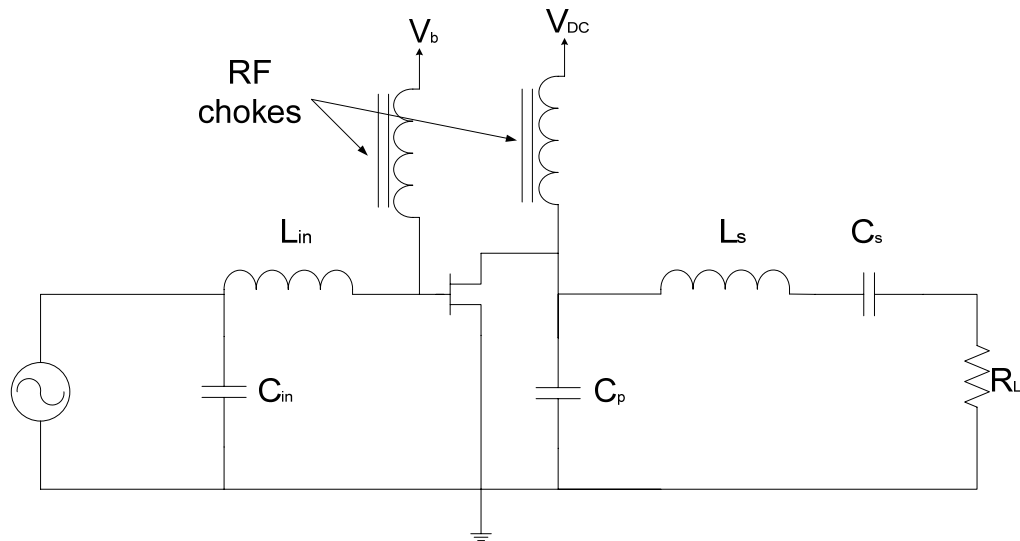


**Figure 2-2: Class-E circuit.**

Transmission lines have been used to provide the matching in class E power amplifiers. Mader and Popovic made in [9] an analysis of a transistor to work as a class E amplifier using transmission lines. First, they reported that the required load impedance is given by:

$$Z_{net} = \frac{0.28015}{\omega_s C_s} e^{j49.0524^\circ} \quad (1)$$

Other important factor to obtain high efficiency is to ensure an open circuit for the second harmonic. To obtain the efficiency and maximum operating frequency they modeled the transistor in the ON and OFF states. In the ON state, the transistor is treated as a constant resistance while at the OFF state the transistor is assumed to be a constant capacitance.

With these assumptions, they reported the efficiency and maximum operating frequency as follows:

$$\eta_d = \frac{1 + \left(\frac{\pi}{2} + \omega_s C_s R_s\right)^2}{\left(1 + \frac{\pi^2}{4}\right) (1 + \pi \omega_s C_s R_s)^2} \quad (2)$$

$$f_{\max} \simeq \frac{I_{\max}}{56.5 C_s V_{ds}} \quad (3)$$

where  $\omega_s$  is the fundamental frequency of operation,  $C_s$  is the switched capacitor which modeled the transistor during the OFF-state,  $R_s$  is the resistance which modeled the transistor during the ON-state,  $I_{\max}$  is the peak output current for the transistor, and  $V_{ds}$  is the bias voltage. To verify their assumptions, they made a comparison at three different frequencies: 0.5 GHz, 1 GHz and 2 GHz. The amplifier maintains a 75% power added efficiency over a 10% bandwidth at 0.5 GHz.

In 1998, a more complete study about microwave power amplifiers was published by Mader, et. al. in [10]. One important assumption made in this paper is a duty cycle of 50% since that it is the optimum case. The equivalent circuit that they used for analyzing the transistor is shown in Figure 2-3.

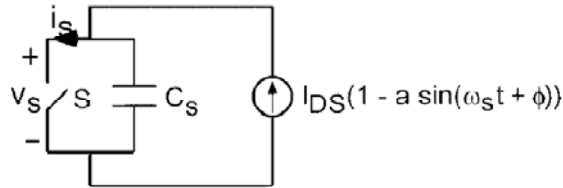


**Figure 2-3: Equivalent circuit for the class-E module. Figure obtained from [10]**

The use of this circuit assumes a zero resistance in the on state, an infinity resistance in the off state and a linear capacitance. From that analysis, they showed that the voltage across the switch is given by:

$$v_s(t) = \frac{I_{DS}}{\omega_s C_s} (\omega_s t + a(\cos(\omega_s t + \phi) - \cos\phi)) \quad (4)$$

where,

$$a=1.862$$

$$\phi=32.48^\circ$$

At this time, they built two class-E amplifiers with different transistors: the Fujitsu FLK052WG and the FLK202MH-14. The last one provides more power but needs five times the input power to operate as class-E amplifier. With the FLK052WG they obtained efficiencies greater than 60% over a bandwidth of 10%. Then, with this amplifier an array was made at a frequency of 5 GHz. The result shows that the combining efficiency is 84%.

A class-E RF amplifiers article was published in 2001 [11]. Some important points about class E amplifiers found in this article are: 1) class A or B amplifiers have approximately 2.3 times more losses than a class E, 2) in a class E there cannot be high voltage and high current at the same time, 3) the transistor acts like a switch. The schematic of the class E amplifier used in this article is shown in Figure 2-4. Increasing C1 the RMS to average current ratio and the peak to average voltage ratio are reduced. Therefore, with lower currents the losses are lower and the efficiency increases. They mentioned that in frequencies below 3 MHz the class D is preferred since the output power is greater, and above 3 MHz the class-E is preferred since it is more efficient.

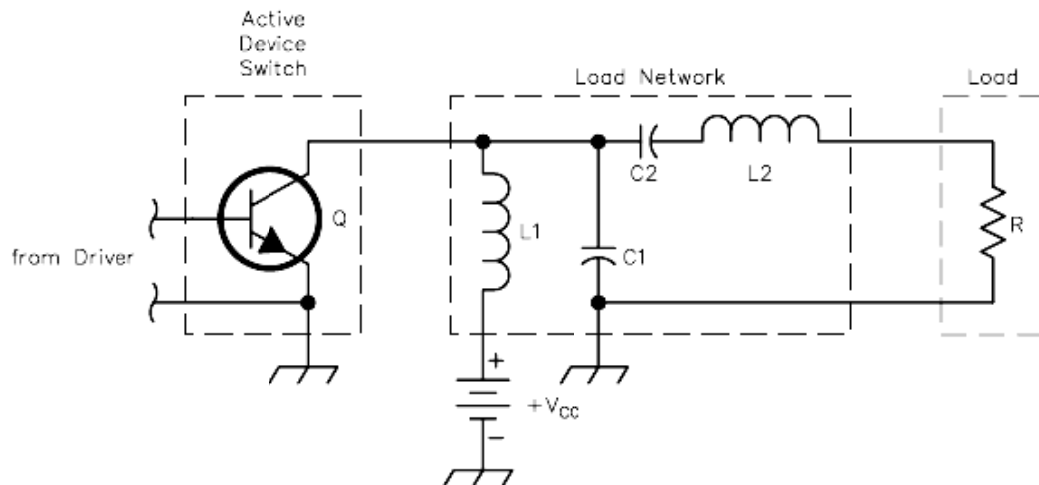


**Figure 2-4: Class-E Amplifier. Figure obtained from [11].**

### 2.3 TAPERED SLOT ANTENNAS

The characteristics of the TSA have made them an interesting research theme since their introduction by Lewis [12] in 1974. Its main advantages are its wideband performance, endfire radiation, symmetric beam, and relatively easy construction. These advantages have converted TSA as an excellent alternative for applications where an implementation with MMIC (Monolithic Microwave Integrated Circuits) is needed [2-5] as well as applications where a wideband array is needed [13-14]

In order to improve these characteristics, different types of tapers have been investigated, such as linear, constant width (CWSA), bunny ear [15], and exponential (Vivaldi) [15-16]. In the case of the Vivaldi, bandwidths of 6:1 have been achieved [15] and antennas as short as one free-space wavelength have been studied [16].

One of the most critical parameters in the design of the TSA is the substrate. Holter, et. al., performed detailed analysis about the substrate effects in TSAs [17]. They showed that the permittivity cannot be very high (greater than 9.8) since the slot mode wavelength,  $\lambda'$ , will be much smaller than the free-space wavelength and, therefore, the fields will be closely confined near the slot, reducing the radiation efficiency [18]. In addition, the slot has to be wide ( $\lambda' \gg 0.6 \lambda_0$ ) for radiation to occur [16]. Consequently, a tradeoff between size and radiation efficiency has to be done. If the main goal is a large efficiency, a thick dielectric with a low permittivity is required. On the other hand, if a short antenna is required, a thin dielectric with a high permittivity must be used. Also, when the thickness is increased the gain is increased [17].

Several authors have investigated the effects of physical parameters, such as opening rate, antenna height, and tapered length on the antenna performance. Research shows that larger opening rates affect negatively the VSWR, although they do not affect the highest and lowest operating frequencies [12-13]. In addition, as the antenna height is decreased, the beamwidth in the E plane is shortened [19]. Finally, a larger antenna has better performance at lower frequencies, but the construction becomes more complicated [13].

Two types of feeding mechanisms have also been studied for TSAs: microstrip and CPW. CPW lines provide larger bandwidth than microstrip [20-21].

Experimental results have been published when permittivity is greater than 9.0 [22] and when permittivity is less than 9.8 [23-24]. One important aspect is that the wavelength and the characteristic impedance of the slot increase when the slot width is increased [16].

When TSAs are used in the design of an array, results show that the antenna performance can change dramatically from its isolated performance. Schaubert, et. al. in dealing with TSA arrays, used a tapered length shorter than one wavelength [25]. In terms of the element spacing, it can be as small as 0.1 wavelengths at the lowest frequency [26] and it should be less than  $\frac{1}{2}$  free-space wavelengths at the highest frequency to avoid grating lobes [20].

## **2.4 TSA IN POWER AMPLIFIER APPLICATIONS**

Tapered slot antennas fit nicely in the design of a spatially combined power amplifier because they are broadband, they produce end-fire radiation and their construction is relatively easy. The end-fire characteristic simplifies the implementation with the Class-E modules since they can be placed in the same plane as the antenna, and, as consequence, the connection between the antennas and the modules is easier. The construction is relatively easy, and, since they have several design parameters (more degrees of freedom), there are more options to find the desired frequency of operation and the desired input impedance.

Several authors [1-7] have used TSAs in a X-band waveguide to design broadband spatial power combiners. In some designs four identical trays, where each tray consists of two input and two output TSAs are used [1]. However, the work is extended to add four [2], and six trays [3] with four input and output TSAs. In those cases, the antennas' dimensions have to be adjusted to fit in an X-band waveguide, which limits the slot width

of the antenna. Therefore, a numerical method [5] was used to obtain the desired input impedance for each design.

## 2.5 WAVEGUIDES

A waveguide is a device that provides a path to guide microwaves. It can operate in several transverse electric (TE) and transverse magnetic (TM) modes. However, assuming that  $a > b$ , the dominant mode is the  $TE_{10}$ . Figure 2-5 shows a rectangular waveguide with the E-field lines for the  $TE_{10}$  mode.

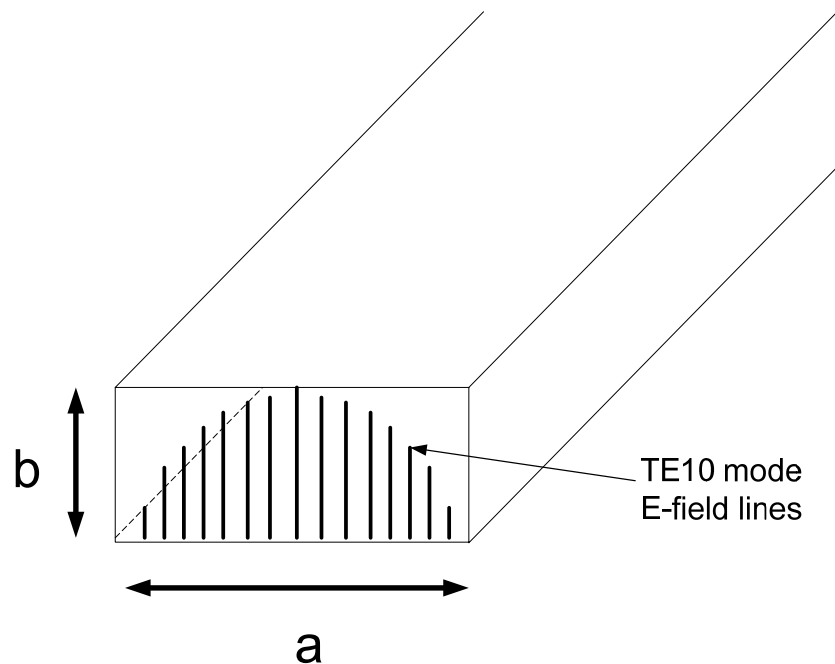


**Figure 2-5: Rectangular waveguide operating in  $TE_{10}$  mode. Appropriate waveguide dimensions are shown as well as the E-field lines for the  $TE_{10}$  mode.**

Once the permittivity and permeability of the material have been fixed, two important parameters establish the cutoff frequency of the guide:  $a$  and  $b$  (length is assumed to be infinite). Given  $a$  and  $b$ , the cutoff frequency can be calculated with Equation 5.

$$(f_c)_{mn} = \frac{1}{2\pi\sqrt{\mu\epsilon}} \sqrt{\left(\frac{m\pi}{a}\right)^2 + \left(\frac{n\pi}{b}\right)^2} \quad (5)$$

where  $mn$  represents the given mode. For the case of an X-band WR90 rectangular waveguide,  $a= 22.86\text{mm}$  (0.9in) and  $b=10.16\text{mm}$  (0.4in). In that case the cutoff frequency for the  $\text{TE}_{10}$  mode is equal to 6.562GHz.

One important point is that the 1 represents an E-Field maximum in the  $a$  dimension and the 0 represents no maximum in the  $b$  dimension. That means that when the  $a$  dimension is increased by  $n$  times there will be  $n$  E-field maxima along  $a$ . The same is applied to  $b$ .

# CHAPTER 3

## METHODOLOGY

The objective of this thesis is to design and implement a Vivaldi antenna array to be used in a high power and high efficiency power amplifier for a solid-state radar. The required output power of the amplifier is 30 W at a frequency of 10 GHz with efficiency better than 70%. This chapter describes each one of the basic steps to achieve this objective in terms of waveguides, antennas, class-E modules and total implementation.

The first step is the selection of the transistor since it will dictate the antenna design. Once it is known, the calculation of the required impedance  $Z_e$  that will allow the amplifier to function as class-E follows. Then, the substrate and its thickness are selected.

The antennas need to be designed to have 50 Ohms at the input of the transistor. There are two options for the output: 1) design antennas with  $Z_e$  impedance, or 2) use 50 Ohms antennas and design a match to obtain  $Z_e$  impedance at the output. One desired characteristic is a harmonic termination at 20 GHz in the antenna design. The reason for doing this is to decrease the power consumption in the harmonics and thus increase the efficiency of the configuration. It is important to select the type of the antennas and the lines to be used to feed them.

Once the antenna impedances are selected, it is fundamental to test the class-E module before it is implemented with the antennas. In this case, it is necessary to check the transistor stability. A circuit for this test needs 50 Ohms lines at the input and output impedance of  $Z_e$ . A network analyzer is required to measure S parameters. If  $S_{11}$  is

greater than 0 dB the transistor is unstable and the next step is to find stability circles and design a matching network out of the unstable region.

When the transistor is stable, it is tested. Input and output power measurements are essential to characterize the amplifier. Figure 3-1 shows the setup to obtain these values with the losses in each component and cable. First, the network analyzer is used to send a 10GHz signal. The signal passes through a pre-amplifier that has a gain of 24dB. A low pass filter is used to block high frequencies. Then, a coupler sends a sample to a power meter in order to calculate the input power to the transistor. Reflections will be measured with the second power meter. A 3 dB attenuator is used to reduce power at the input of the class-E module and not damage the transistor. At the output of the amplifier, a 30dB attenuator reduces the power to eliminate the risk of damaging the last power meter. This power meter provides the output power of the class-E module. With these values, efficiency and gain are calculated.

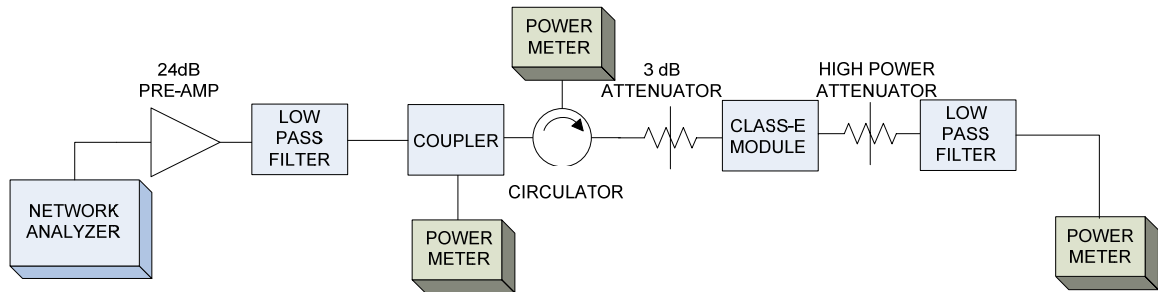


**Figure 3-1: Setup to test the class-E module. Input and output powers are measured.**

The final design requires an overmoded waveguide. In this design, a transition from a  $TE_{10}$  mode to the  $TE_{30}$  has to be made. The main restrictions are a low reflection coefficient at the input (less than -10dB) and a high transmission coefficient (approximately 0dB).

Finally, after all the components are designed, the implementation of the space distributed amplifier is needed. Testing for output power given an input power must be done and efficiency must be calculated with power values.

# CHAPTER 4

## DESIGN PROCEDURE

The design of the power amplifier consists of four different stages: 1) waveguide design and its transitions, 2) tapered slot antennas, 3) class-E modules, and 4) total implementation. In this chapter, these concepts are explained.

### 4.1 WAVEGUIDE

#### 4.1.1 FIRST DESIGN

To accommodate more trays, a waveguide operating at the  $TE_{30}$  mode was designed. This configuration permits three trays to be placed at E-field maxima (see Figure 4-1) increasing the power generated by the amplifier. The dimensions for the  $TE_{10}$  and  $TE_{30}$  modes at 10 GHz are shown in Table 4-1.

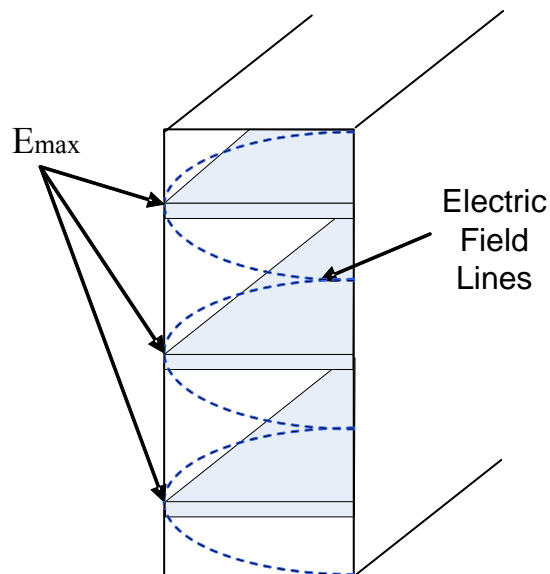


**Figure 4-1: Configuration of the trays inside the over-mode waveguide. The dashed lines represent the electric field lines and the trays are placed at the E-Field maxima.**

The key in the waveguide design requires selection of a good transition between the TE<sub>10</sub> and the TE<sub>30</sub> modes. To do this, the distance between the TE<sub>10</sub> waveguide and the TE<sub>30</sub> was increased until a low reflection coefficient (less than -10dB) and a high transmission coefficient (approximately 0dB) were obtained. Figure 4-2 shows the physical design of the waveguide.

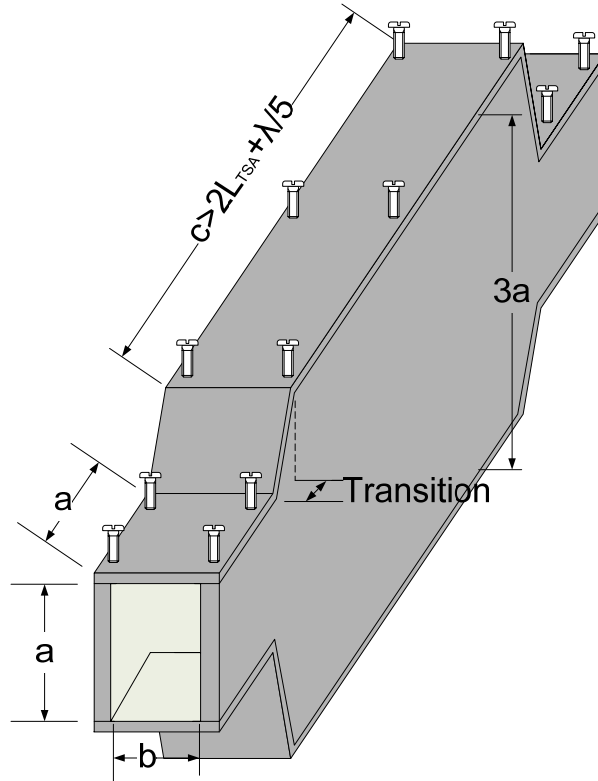


**Figure 4-2: Waveguide design. Transition between TE<sub>10</sub> and TE<sub>30</sub> dimensions is presented.**

**Table 4-1: Transversal electromagnetics modes for the 10 and 30 modes at 10GHz. The a and b dimensions for these modes are shown in mm. Dimension c used is also shown.**

Mode	a(mm)	b(mm)	c(mm)
TE <sub>10</sub>	22.86	10.1	22.86
TE <sub>30</sub> (First Design)	68.58	10.1	90.86
TE <sub>30</sub> (Second Design)	68.58	10.1	125.45

### 4.1.2 SECOND DESIGN

The waveguide dimensions had to be changed since the tray configuration changed. The configuration change was due to the addition of the matching network (that will be explained in a next section) and the increase in the distance from the waveguide transition to the antennas. As Table 4-1 shows, the new waveguide design is larger than the first. In addition, two metal sheets were added inside the waveguide to force the three E-field maximum. The design simplifies the assembly at the same time that takes into account the bias of the transistors (see Figure 4-3).

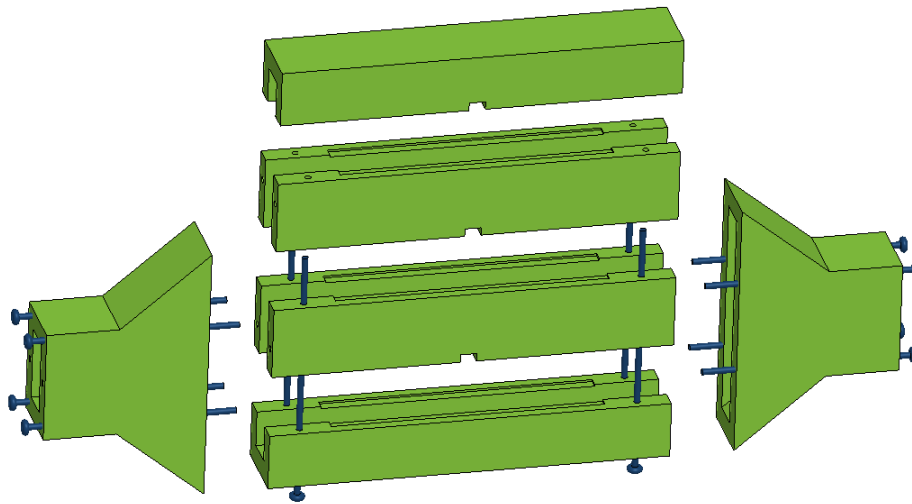


**Figure 4-3: Second waveguide design is presented. This design is larger than the first one and takes in account the place to bias the transistors.**

## 4.2 TAPERED SLOT ANTENNAS

### 4.2.1 SUBSTRATE SELECTION

The substrate was selected to obtain a short antenna. Since a wideband operation was not a requirement in this application, the bandwidth can be sacrificed in order to reduce the antenna length. Therefore, a relatively high permittivity ( $\epsilon_r=6.15$ ) substrate (Rogers RT/Duroid 6006) with a thickness of 0.635 mm was used for the design.

### 4.2.2 FEED TYPE

Coplanar waveguide transmission (CPW) line was selected to make the placing of the solid-state devices simpler. In addition, CPW gives a broader bandwidth than microstrip. Another advantage of this transmission line is that the substrate does not require backside processing since this side has no metal.

### 4.2.3 ANTENNA GEOMETRY

Four TSAs were designed in each tray. The Vivaldi antennas were used in this analysis and the curve was modeled using (6).

$$L = \frac{W_{feed}}{2} e^{-\Delta \times l} \quad (6)$$

$W_{feed}$  is the width at which the antenna starts to open,  $\Delta$  is the rate at which the curve increases, and  $l$  is the position in the antenna length. The tray configuration is shown in Figure 4-4.

One of the goals of the research is to design low impedance output antennas (maximum 24  $\Omega$ ) and 50  $\Omega$  input impedance antennas. However, with the available equipment to build the transmission lines and antennas, it is not possible to make the required slots for these impedances. Therefore, we focused our work in the design of 65  $\Omega$  input impedance antennas, and applied the obtained knowledge in the design of the 24  $\Omega$  and 50  $\Omega$  antennas.

CPW lines have 65  $\Omega$  impedance, as well as the antenna input impedance, and the port impedance. The slot width at the open end of the antennas was limited by the inner dimension of the waveguide,  $b$ , (in this case  $b=10.1\text{mm}$ , as shown in Figure 4-4). To increase the input impedance of the center antennas, their open end is wider than the open end of the edge antennas.

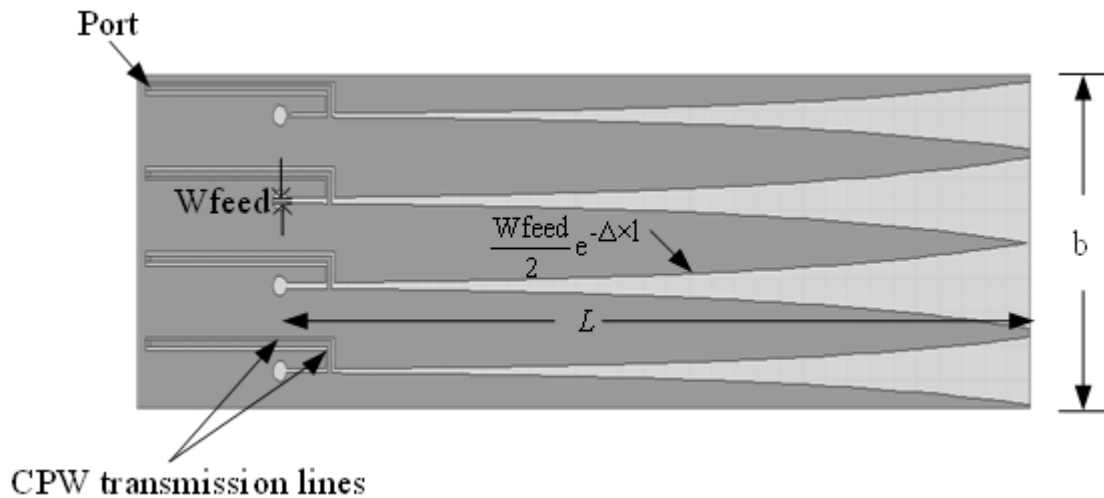


**Figure 4-4: Tray configuration.**

The radius of the open-circuit circle at the feed end was analyzed to obtain the best VSWR. The best value was around 0.3 mm; as the radius is increased, the VSWR at mid-band frequencies increases

#### **4.2.4 ANTENNA GEOMETRY- SECOND DESIGN**

One of the main specifications at the time of designing a high efficiency amplifier is to take in account the harmonics in order to avoid power consumption at these frequencies. The best solution to this problem is to design an open or short circuit stub at those frequencies. However, it is not possible to design a stub for all harmonics. Commonly, only the second harmonic is selected since it consumes the greatest amount of power. Since the goal of this research is to have an operational frequency of 10 GHz, a short circuit stub at 20GHz (second harmonic) decreases significantly the power consumption.

For this reason, once the design of the antenna was obtained, a short circuit stub was added to increase the VSWR at 20 GHz. Figure 4-5 shows the stub design. Because of the stub effects, the antenna dimensions have to be changed in order to maintain a good bandwidth at 10 GHz.

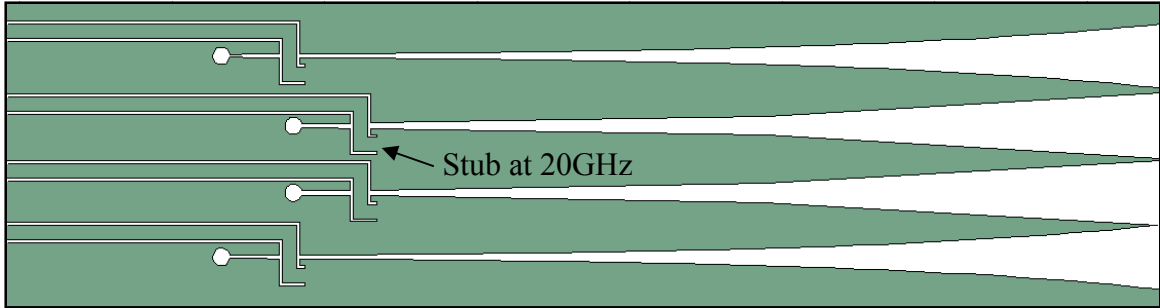


**Figure 4-5: The tray configuration is shown. A short circuit stub is added to the antennas to create a mismatch at 20 GHz.**

### 4.3 CLASS-E AMPLIFIER

The first step to design the class E amplifiers was to select transistors that operate at least until 20 GHz. In this selection process the available ones were from Triquint Semiconductor and from Alpha Industries. The load impedance needed for each one to operate as class-E was calculated and the values are shown in Table 4-2. This table also shows the maximum output power for each one.

**Table 4-2: Available transistors are shown. Transistors required impedance to operate as class-E and the maximum output power are displayed.**

TRANSISTOR	IMPEDANCE	OUTPUT POWER (DBM)	OUTPUT POWER (W)
AFM04P2-000	1.88-j2.17	21	0.125
TGF2022-06	25.40+j29.28	28	0.631
TGF2022-12	12.7+j14.64	31	1.259
TGF2022-24	6.35+j7.32	34	2.512
TGF2022-48	3.18+j3.66	37	5.012
TGF2022-60	2.55+j2.94	38	6.309

From this table, noted that, for Triquint transistors the output power increases as the impedance decreases. Therefore, a tradeoff between output power and impedance had to be made. For this research, the transistors used were TGF2022-12.

After the transistor was selected, a circuit to prove its performance was built (see Figure 4-6). For this transistor, the maximum drain to source voltage is 12V which means that the maximum voltage that can be applied to acts as class-E is 3.51 V.

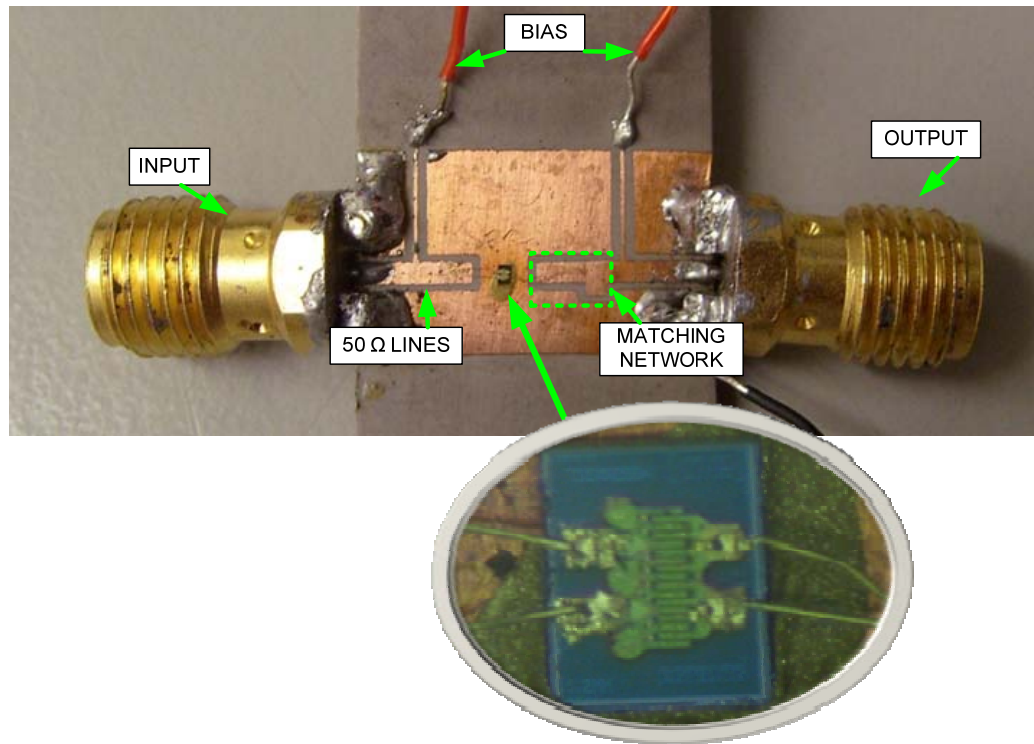


**Figure 4-6: Transistor circuit is shown. The bias and matching networks as well as the gate and drain connections are shown.**

The setup showed in Figure 4-7 was done to test the class-E module. Losses in this circuit were measured to characterize the setup and are presented in Figure 4-8.

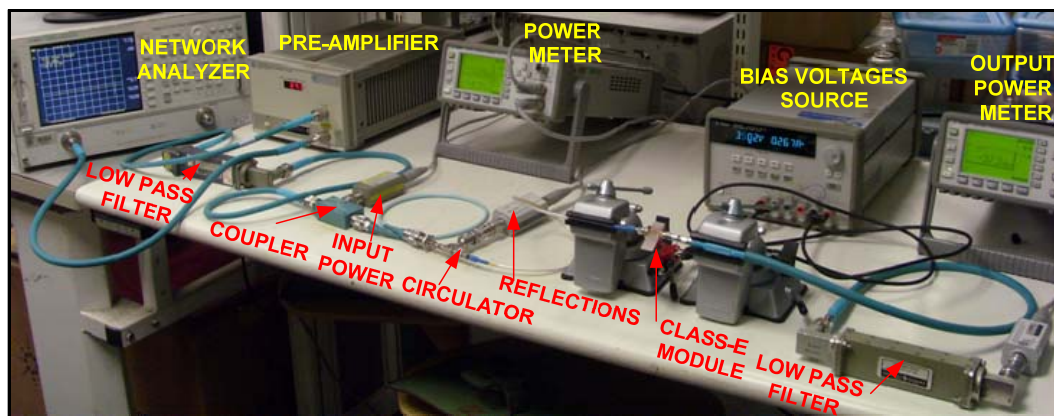


**Figure 4-7: Setup to test the class-E module.**

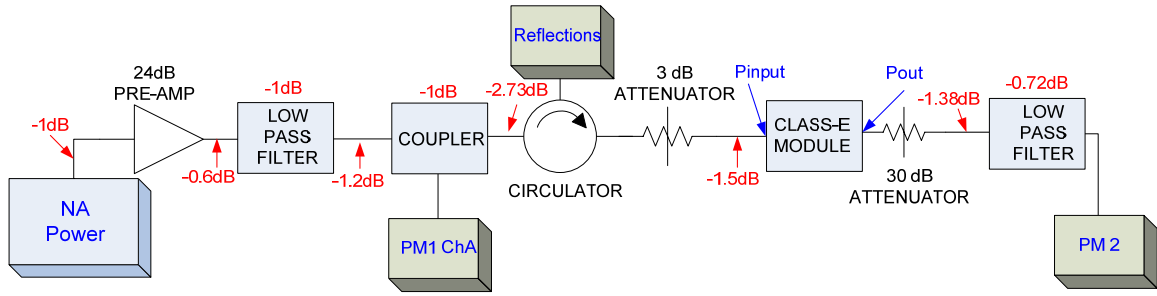


**Figure 4-8: Setup to test the amplifier. Losses in each component and in cables are presented in red. Measured and calculated powers are presented in blue.**

With the measured losses in cables and components, the delivered power to the class-E module can be calculated as:

$$\begin{aligned}
 P_{delivered} &= PMChA(dBm) + C - IL_{coupler} - L_{cable} - L_{circulator} - 3dB_{attenuator} \\
 &\quad - L_{cable} \\
 &= PMChA(dBm) + 20dB - 1dB - 2.73dB - 0dB - 3dB - 1.5dB \\
 P_{delivered} (dBm) &= PMChA(dBm) + 11.77dB
 \end{aligned} \tag{7}$$

It is needed to subtract the reflections at the input to obtain the input power. To obtain these reflections, a power meter is included in the setup. However, this measurement includes a part of the power that passes through the circulator. Therefore, the real reflected power measured can be obtained as:

$$P_{refmed}(W) = Reflections (W) - PinCirIL(W) \tag{8}$$

where

$$\begin{aligned}
 PinCirIL(dBm) &= PMChA(dBm) + C - IL_{coupler} - L_{cable} - IL_{circulator} \\
 &= PMChA(dBm) + 20dB - 1dB - 2.73dB - 20dB \\
 &= PMChA(dBm) - 3.73dB
 \end{aligned} \tag{9}$$

Since these are the measured reflections, the reflected power at the input of the class-E module is obtained adding the reflections path losses to Equation (8):

$$P_{ref}(dBm) = P_{refmed}(dBm) + 3dB_{attenuator} + L_{cable} \quad (10)$$

Once this power is obtained, the input power to the class-E module is calculated as:

$$P_{input} = P_{delivered}(W) - P_{ref}(W) \quad (11)$$

The output power is calculated as:

$$\begin{aligned} P_{out} &= PM2 + L_{Filter} + L_{cable} + 30dB_{attenuator} \\ &= PM2 + 0.72dB + 1.38dB + 30dB \\ P_{out}(dBm) &= PM2 + 32.1 \end{aligned} \quad (12)$$

With these two values the gain of the amplifier can be calculated with the following equation:

$$G(dB) = P_{out}(dBm) - P_{input}(dBm) \quad (13)$$

The drain-source current has to be measured to calculate DC input power. Once this power is obtained, the drain efficiency and the power added efficiency (PAE) as:

$$\eta = \frac{P_{out}(W)}{P_{dc}(W)} \quad (14)$$

$$PAE = \frac{P_{out}(W) - P_{input}(W)}{P_{dc}(W)} \quad (15)$$

## 4.4 MATCHING AND BIAS NETWORKS

### 4.4.1 MATCHING NETWORK

Since it was not possible to build the low impedance antennas with the available equipment, 50 Ohms antennas were used to the input and output of the class E amplifiers. However, given that the transistor needs low output impedance (in this case approximately 12+j14 Ohms) to operate as a class-E amplifier, a matching network had to be designed to change the impedance from 50 Ohms to the desired impedance.

A single stub tuning with a short circuit was selected. The principal advantages of this technique are that no lumped elements are required and are easy to fabricate with CPW. Figure 4-9 shows the matching network equivalent circuit and the CPW implementation.

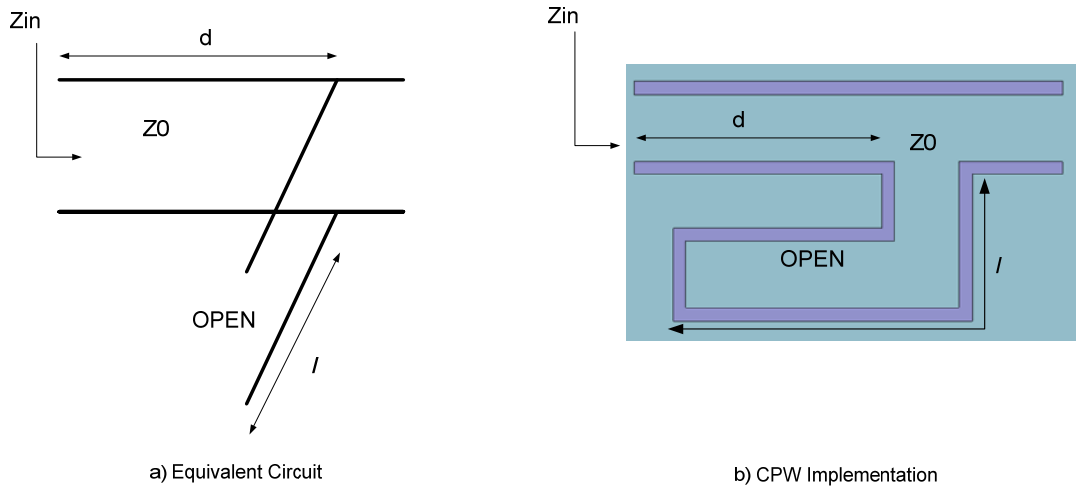


**Figure 4-9: Matching network with an open stub. The figure presents the a) equivalent circuit and b) CPW implementation for the matching network.**

#### 4.4.2 BIAS NETWORK

Since there is no available space to implement a high frequency choke, the bias network was implemented with inductors of 2.7 nH (see Figure 4-10).

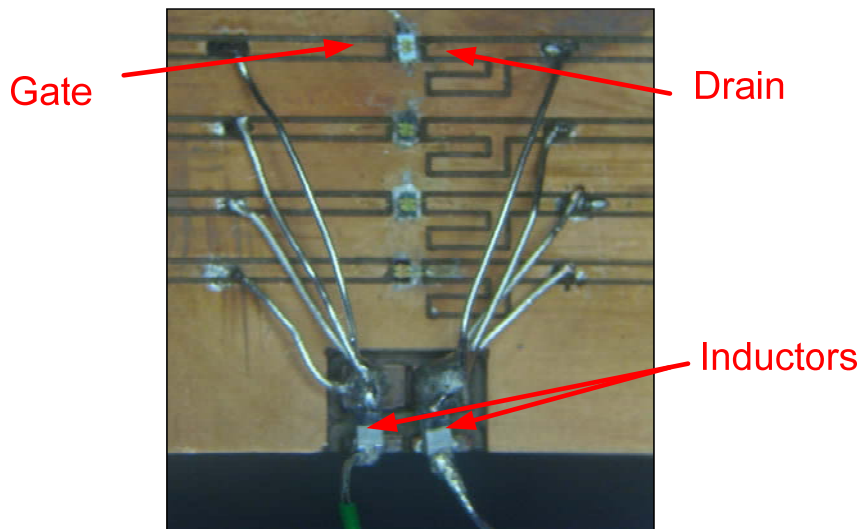


**Figure 4-10: Bias Network. Gate and drain bias connections are shown.**

## 4.5 SPATIALLY DISTRIBUTED AMPLIFIER

Once each part was proved separately, the final tray to the proposed distributed amplifier was designed (see Figure 4-11).

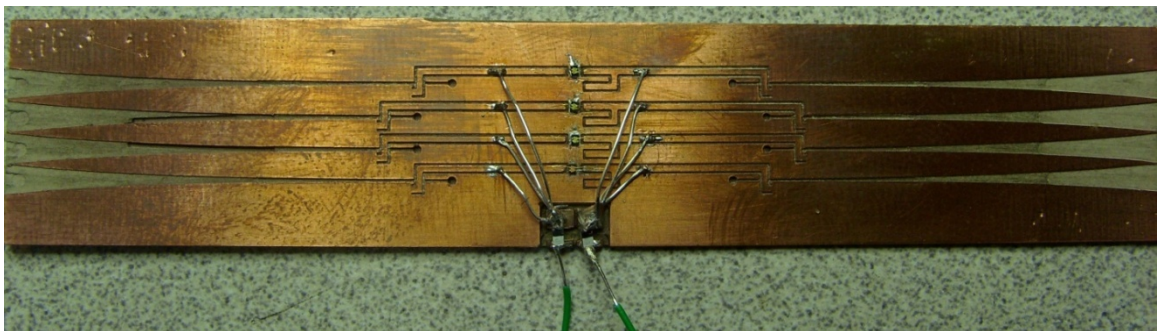
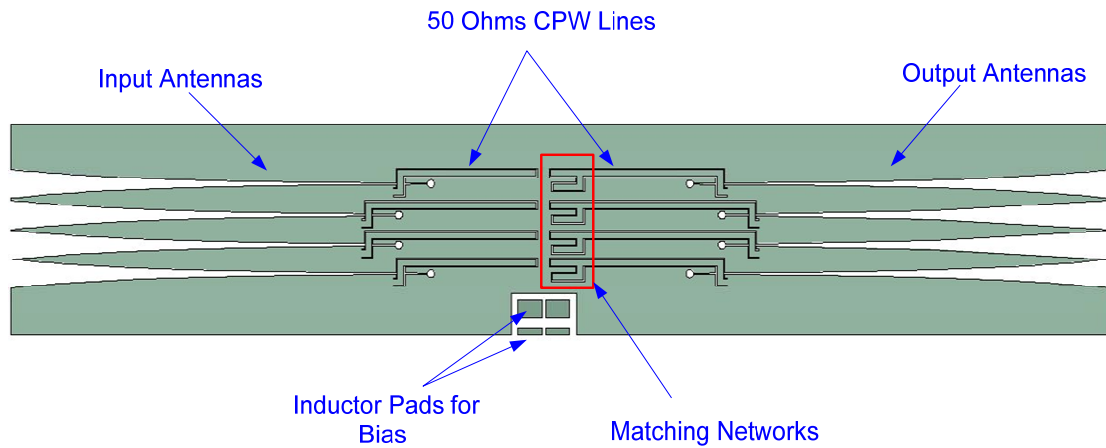


**Figure 4-11: Complete tray design.**

# CHAPTER 5

## RESULTS

This chapter presents simulated and measured values for the waveguides. Then, antennas for 65 Ohms, 24 Ohms and 50 Ohms are shown. Results of harmonic terminations, matching networks and bias networks are described. The class-E module results are also explained.

### 5.1 WAVEGUIDE

#### 5.1.1 WAVEGUIDE- FIRST DESIGN

Simulations in Ansoft HFSS showed that the best performance at 10GHz was obtained with a transition of 28mm. With this dimension the  $S_{11}$  and  $S_{22}$  parameters are less than -30 dB meaning a low reflection coefficient. At the same time, an excellent transmission coefficient was achieved with a  $S_{12}$  and  $S_{21}$  near 0dB.

Once the simulations achieved the desired performance, the waveguide was built. S parameters were measured with an Agilent 8719ES network analyzer. Figure 5-1 shows measured and simulated s parameters for the waveguide. The difference in simulated and measured values of  $S_{21}$  and  $S_{12}$  is approximately 0.5 dB. In the cases of  $S_{11}$  and  $S_{22}$  difference is greater. However, the measured values for all parameters were adequate at 10 GHz. Differences between simulated and measured values were due to the accuracy of the physical construction of the waveguide.

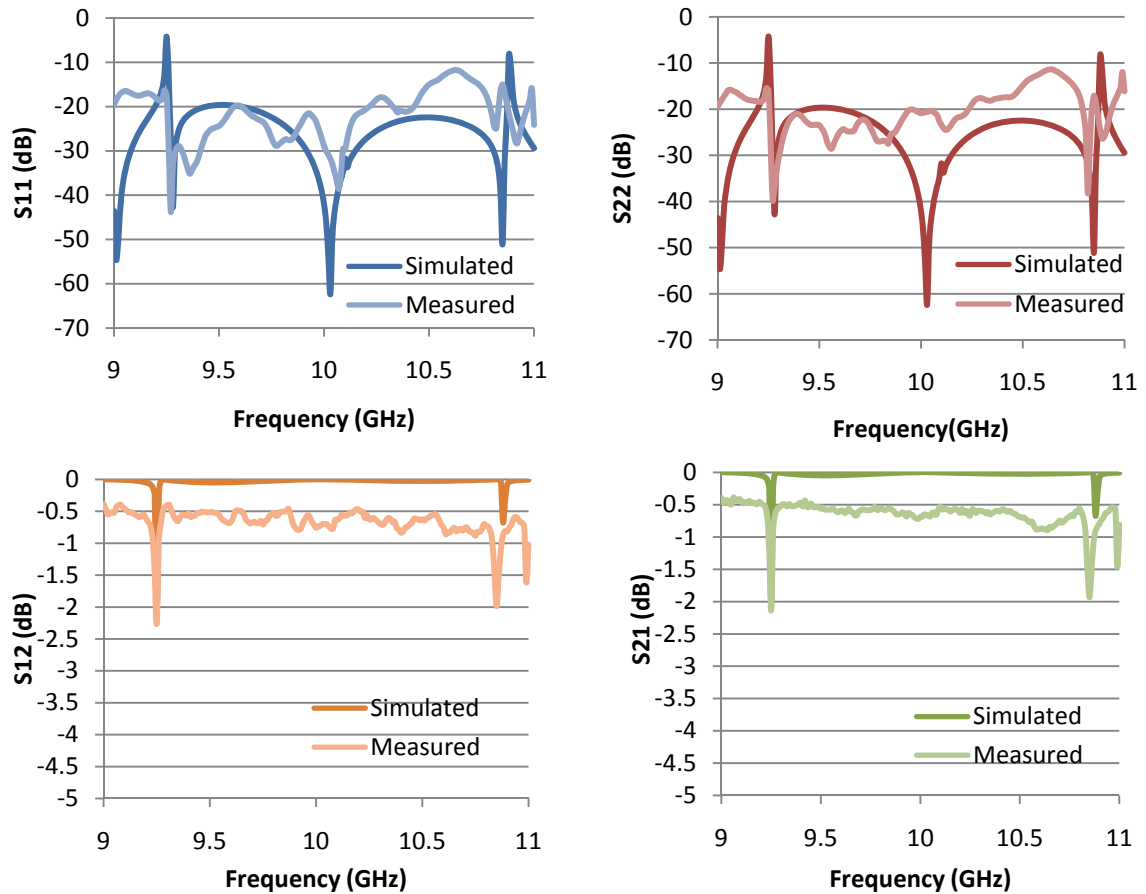


**Figure 5-1: S parameters for the overmoded waveguide. Simulated and measured values for S11, S12, S21 and S22 are shown.**

### 5.1.2 WAVEGUIDE- SECOND DESIGN

For the final design the length of the waveguide had to be increased in order to place the amplifiers and the input and output antennas. However, the transition between the two modes was maintained constant. In addition to this change, two metal sheets were added to force E-field maxima. To verify it, a simulation was made and the results are shown in Figure 5-2. In this, it can be seen that three maximums are formed in the waveguide.

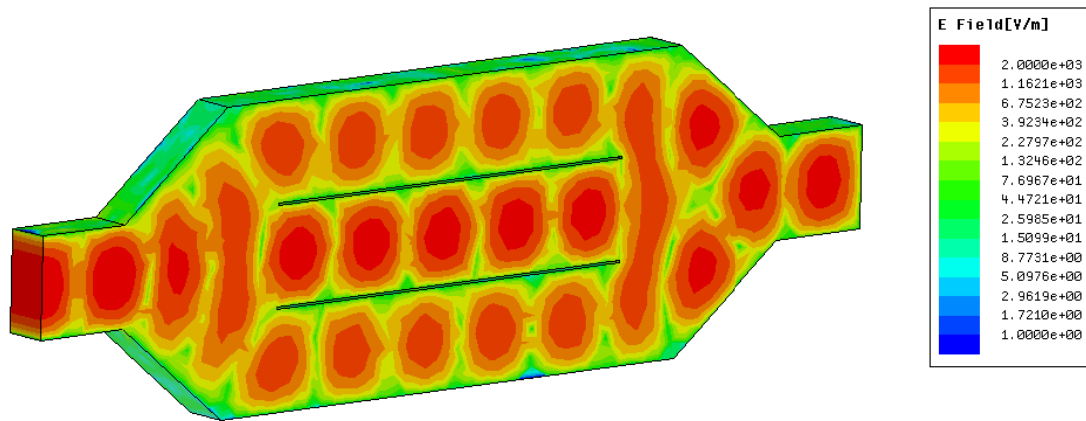


**Figure 5-2: E-fields amplitude inside the waveguide. The figure shows that three maximums are formed inside the waveguide.**

After that, S-parameters were measured to compare it with simulations (see Figure 5-3). Figure 5-4 shows measure and simulated values for this waveguide.

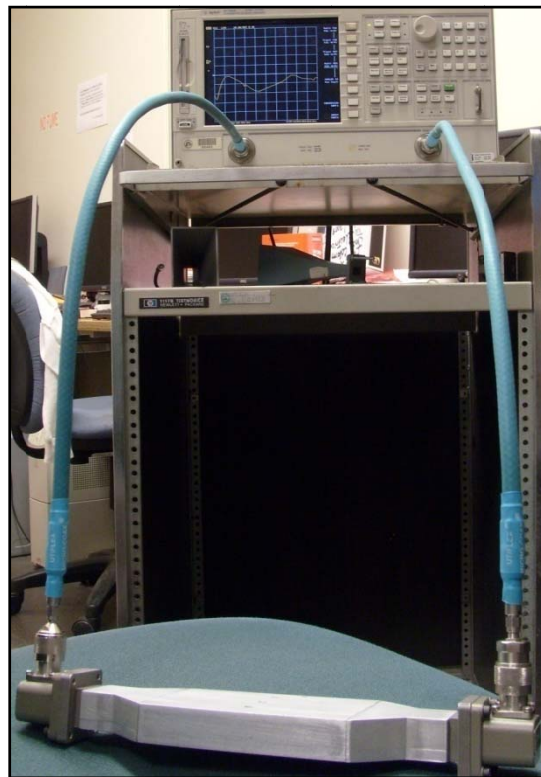


**Figure 5-3: Setup to measure waveguide S parameters. The network analyzer shows input port reflections.**

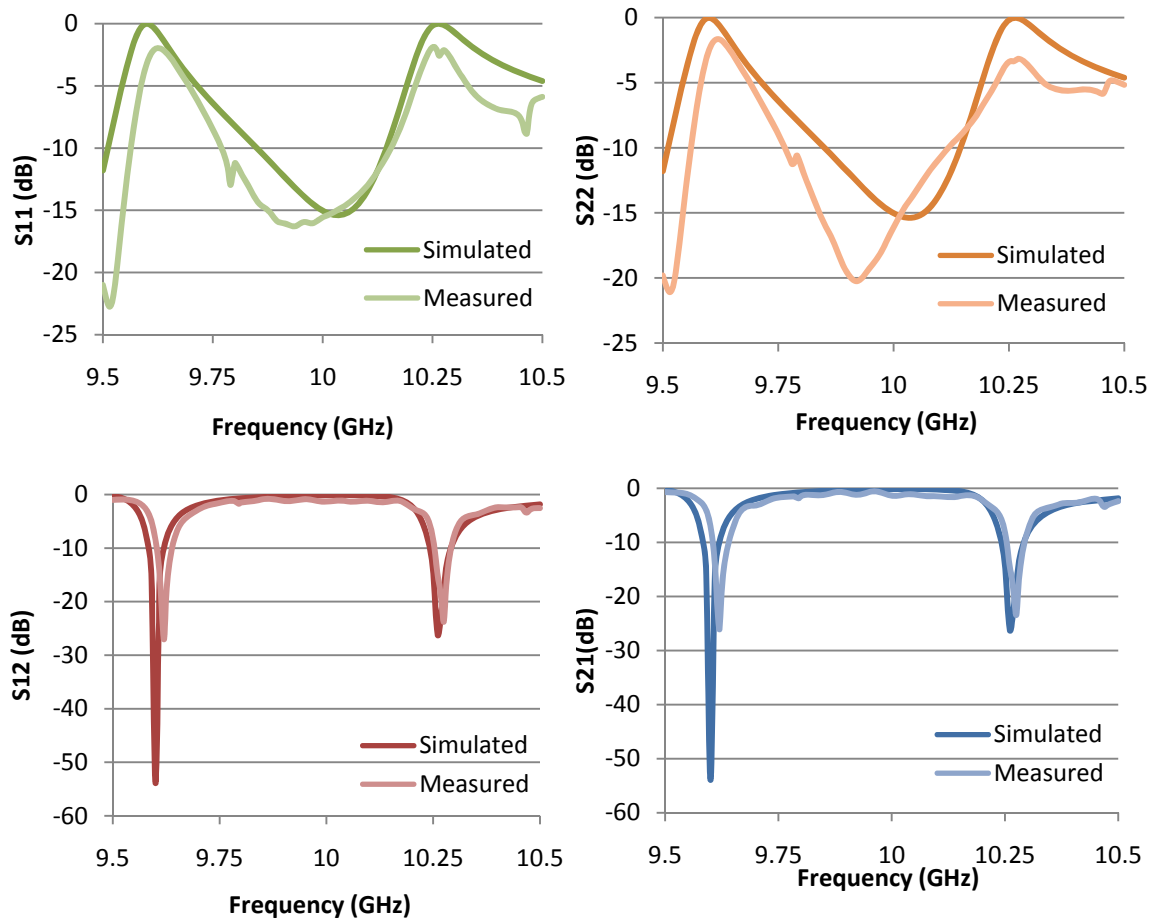


**Figure 5-4: S parameters for the second waveguide design are shown.**

These results show that measure values of  $S_{11}$  and  $S_{22}$  have differences from the simulated ones. It is due to calibration since the waveguide to N connector is not taken in account when the calibration was done. Parameters  $S_{12}$  and  $S_{21}$  show a great similitude with the simulated values.

## 5.2 ANTENNAS

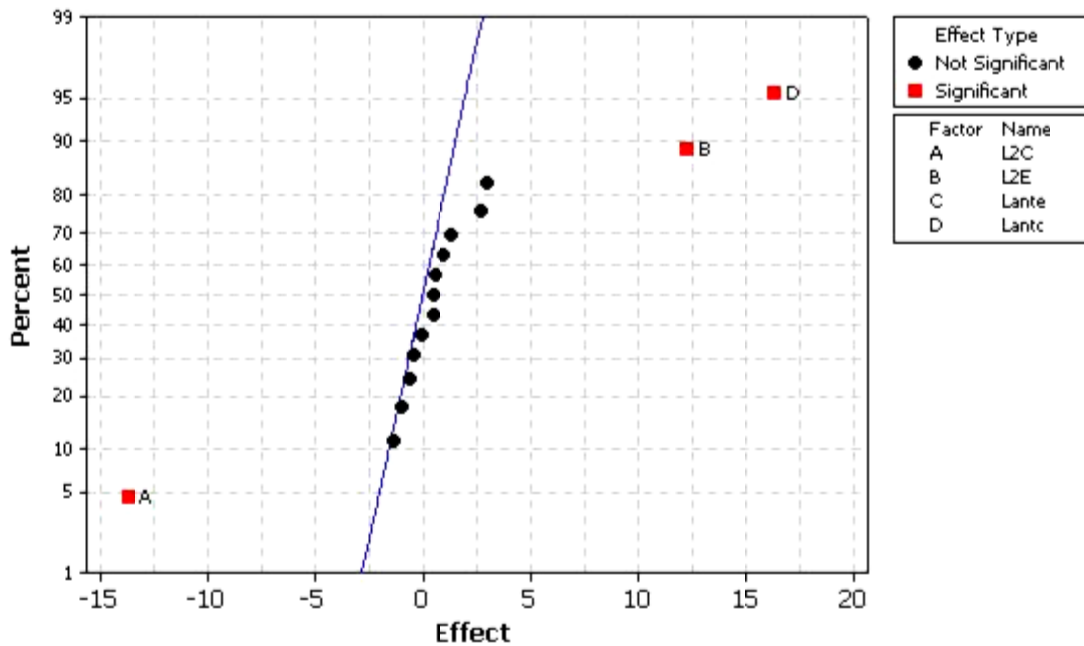
### 5.2.1 DESIGN OF EXPERIMENT (DOE)

A Design of Experiments was applied to the 65  $\Omega$  antennas to determine how the performance of the antenna changes with changes in the design parameters. To limit the size of the problem, trays were kept identical; that is, the antenna dimensions are the same for each tray. By doing this, 4 variables are left: 1) the length of the center antennas

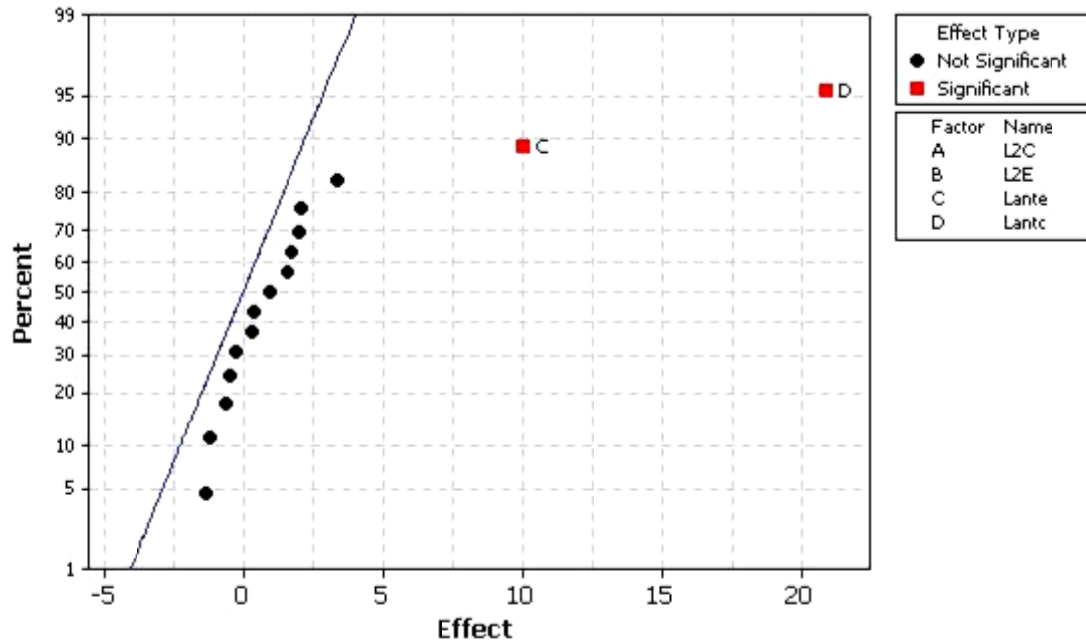
( $L_{antc}$ ), 2) the length of the edge antennas ( $L_{ante}$ ), 3) the feed point of the edge antennas ( $L_{2e}$ ), and 4) the feed point of the center antennas ( $L_{2c}$ ). The results of the DOE were analyzed to obtain the effects of each variable. The results of this analysis are shown in Figure 5-5 and Figure 5-6.

From these results, the major effects in the impedance can be established as follows:

1. Increasing the distance where the center antennas are fed decreases the resistance of the edge antennas.
2. Increasing where the edge antennas are fed increases the resistance of the edge antennas.
3. Increasing the length of the edge antennas increases the resistance of the center antennas.
4. Increasing the length of the center antennas increases the resistance of the edge and the center antennas.



**Figure 5-5: Significance of the effects of the design parameters in the edge antennas input impedance. Significant parameters and interactions are displayed with a square.**



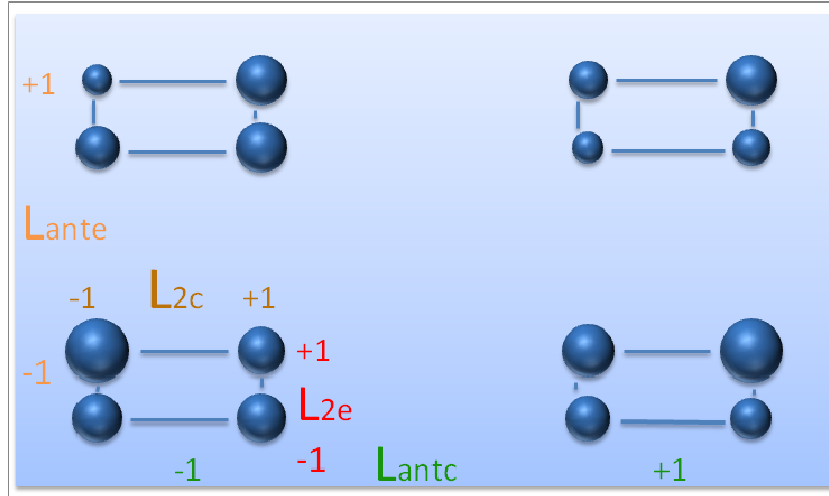
**Figure 5-6: Significance of the effects of the design parameters in the center antennas input impedance. Significant parameters and interactions are displayed with a square.**

Figure 5-7 show the analysis of combinations in terms of the bandwidth. The -1 and +1 represent the low and high values used for each variable. The size of the spheres represents the bandwidth for each one of the sixteen combinations. The larger the size of the sphere the wider the bandwidth. That means that there are two combinations that provide a wide bandwidth:

1. Low values in L2c, Lantc and Lante, and high value in L2e.
2. Low value in Lante, and high values in L2c, L2e and Lantc.

### 5.2.2 BEST PERFORMANCE WITH THREE TRAYS

From the DOE, one of the configurations with larger bandwidth mentioned above was selected. Dimensions are shown in Table 5-1. Figure 5-8 shows the impedance real and imaginary parts, respectively. Note that, in Figure 5-9, all the antennas from 9.90 to 10.21 GHz have a VSWR smaller than two. This gives a bandwidth of 310 MHz, which is adequate for the power amplifier application. In this range, the real part is near  $65 \Omega$  and the imaginary part is close to zero.



**Figure 5-7: Experiment with a four variable factorial design. The -1 and +1 values represent low and high values for each variable, respectively. The size of the spheres represents the bandwidth for each combination of variables. As greater the size, wider the bandwidth.**

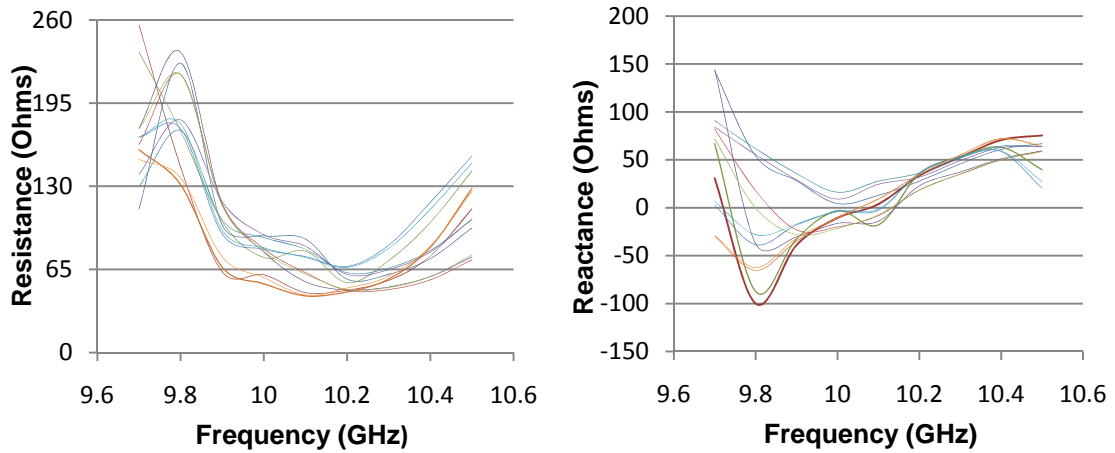


**Figure 5-8: Input resistance and reactance for the 65  $\Omega$  antennas. All the 12 antennas (4 in each of the 3 trays) are displayed.**

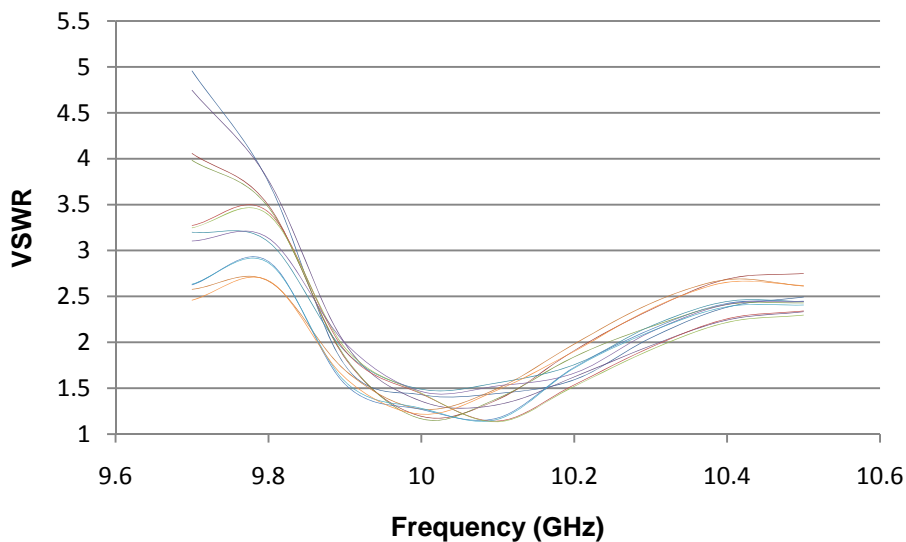


**Figure 5-9: VSWR for the 65  $\Omega$  antennas. All the 12 antennas (4 in each of the 3 trays) are displayed.**

### 5.2.3 MEASURED RESULTS

We built and tested the three-trays configuration to validate the simulated results (see Figure 5-10). The trays were built by wet etching, and placed inside the waveguide. The antenna feed lines were connected to a SMA connector through a wire bond, and both ends of the waveguide were properly terminated. To simplify the connections, only the impedance of the edge antennas on each tray were measured, and terminated the center antenna feed lines with 65  $\Omega$  resistors.

Figure 5-11 shows the VSWR for an edge tray antenna. The measured results are similar to the simulation, although the VSWR is higher in the middle of the bandwidth. The difference is mostly due to the effect of the wire bonding between the antenna feed and the SMA connector.

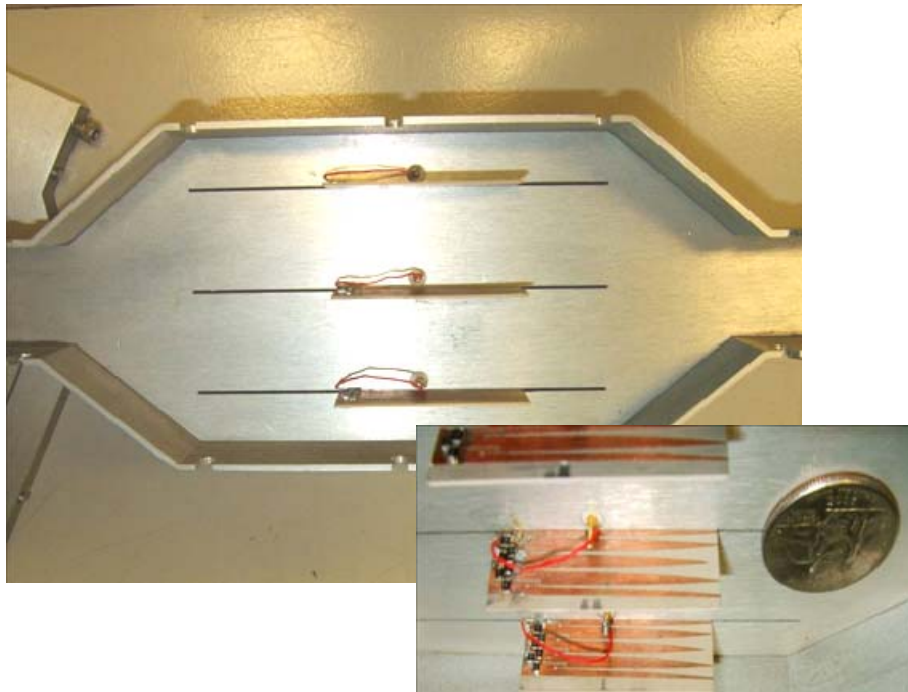


**Figure 5-10: Design setup to measure antennas VSWR and wire bond connection from the antenna feed to the input SMA connector.**

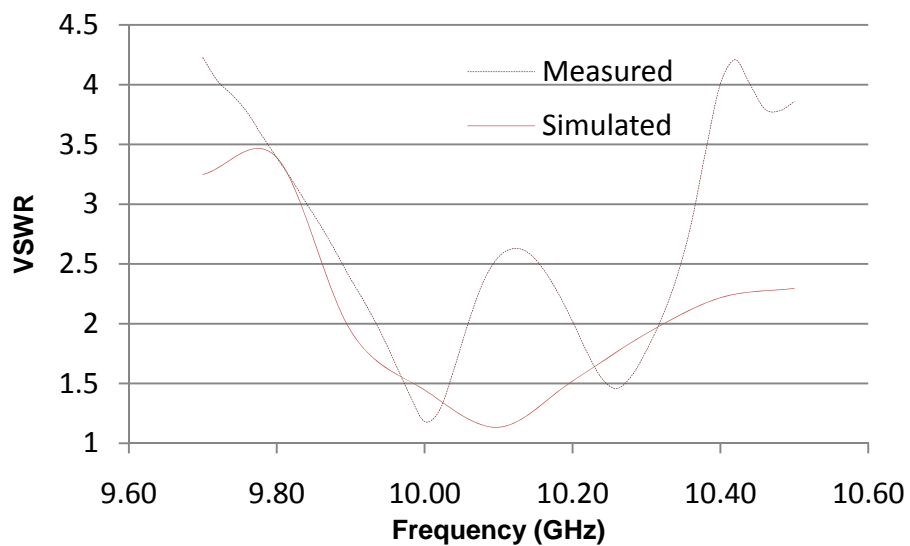


**Figure 5-11: VSWR for an edge antenna on an edge tray. The difference between the measured (blue line) and simulated (red line) is due to the wire from the antenna feed to the input SMA connector.**

#### 5.2.4 SIX AND NINE TRAYS

Once the behavior of the three-trays system was analyzed, more trays were added to see how coupling affects the additional trays. First, three trays were added and all trays were accommodated at 0.9 of the maximum E-field (see Figure 5-12).

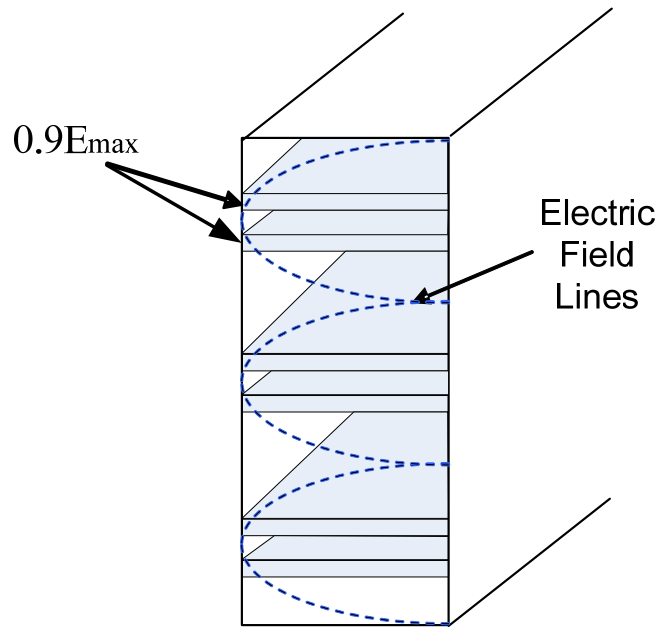


**Figure 5-12: Six trays configuration.**

Simulations show that the additional trays shift the frequency range upwards. However, they have good performance around 10 GHz. Figure 5-13 show the VSWR for this configuration.

After that, three more trays were added. In this configuration, three trays were placed at the E-field maxima and the other six at 0.707 of the maximum as shown in Figure 5-14. VSWR result for this configuration is shown in Figure 5-15.

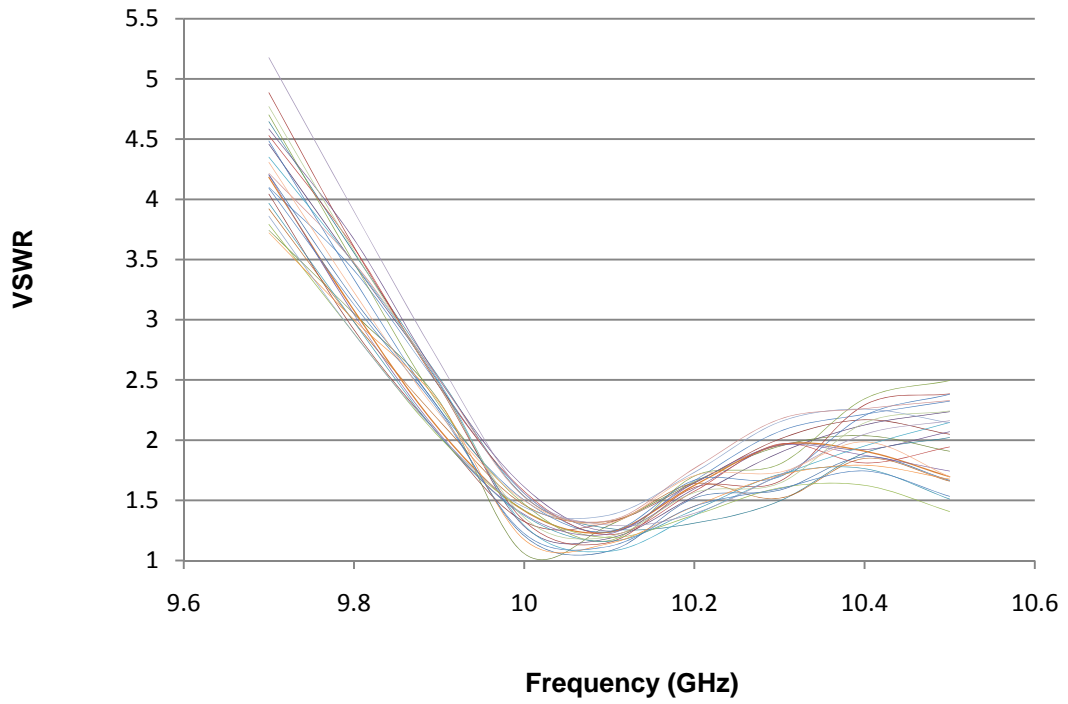


**Figure 5-13: VSWR for the six trays configuration. The results for all 24 antennas are displayed. The trays are placed at the 0.9 of the E-field maxima in the waveguide.**

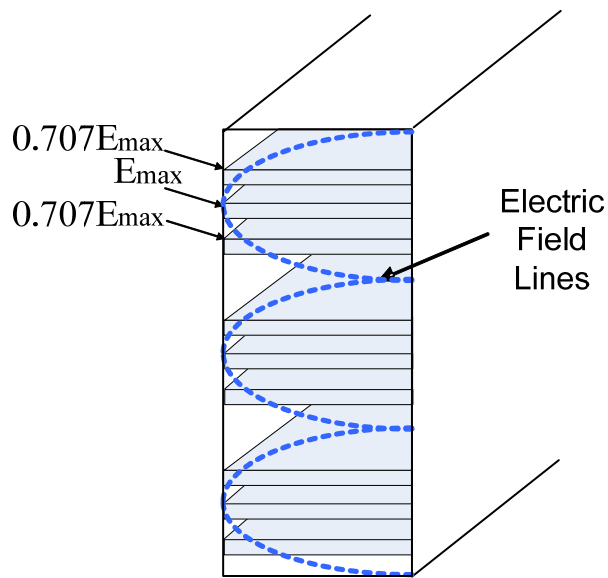


**Figure 5-14: Nine trays configuration.**

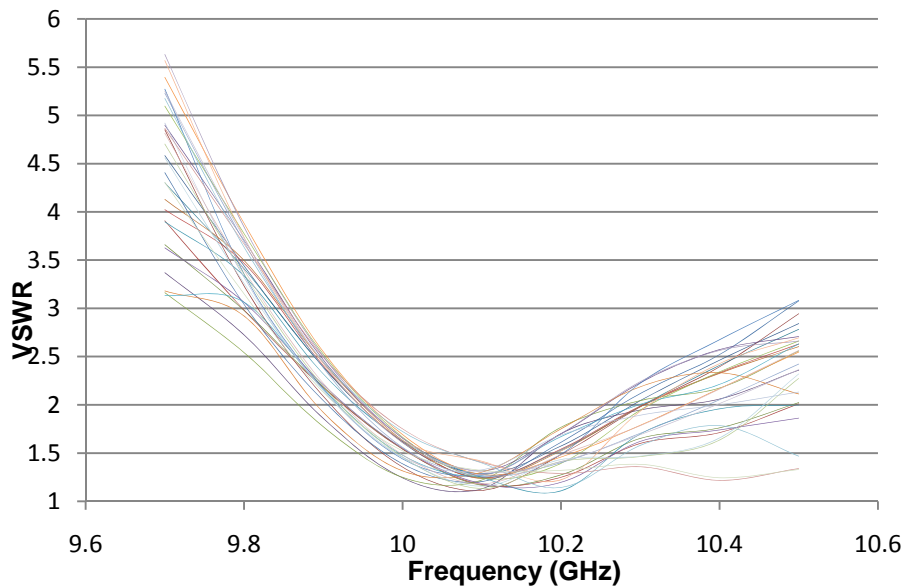


**Figure 5-15: VSWR for the nine trays configuration. The results for all 36 antennas are displayed. The trays are placed at the maximum and the half power points for each of the E-field maxima in the waveguide.**

In both cases, the bandwidth is approximately 300 MHz. Comparing the performance of the three, six and nine-trays configurations, it was found that the performance of the antennas does not change much as the numbers of trays is increased. The center frequency is shifted upwards only 3MHz and the bandwidth is reduced by 3 MHz.

### **5.2.5 INPUT ANTENNAS- 50 $\Omega$ INPUT IMPEDANCE**

The results obtained with the simulations of the 65  $\Omega$  antennas showed that the behavior of the antennas did not change much going from 3 to 9 trays. Therefore, efforts were concentrated in the design of the 50  $\Omega$  antennas, using the 3-tray configuration. The final design dimensions are shown in Table 5-1. Figure 5-16 and Figure 5-17 show the simulated results for the input impedance and VSWR. A 300 MHz bandwidth was obtained for this case.

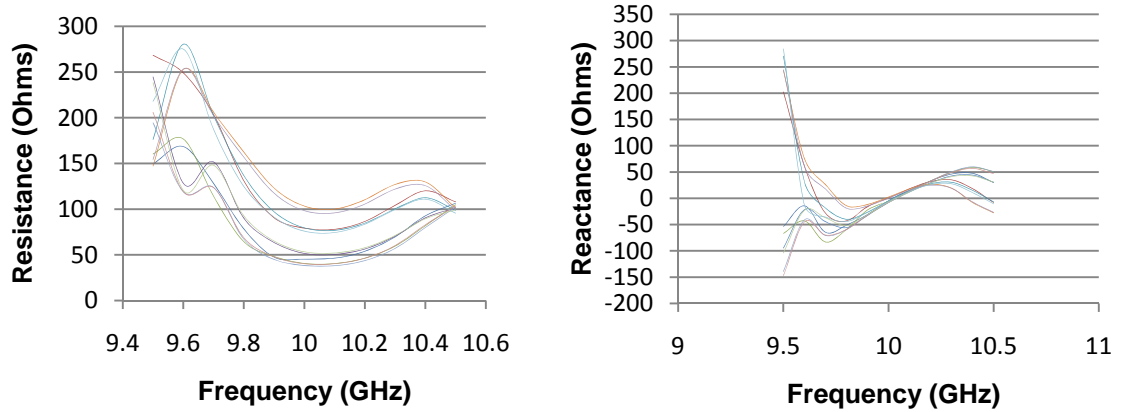


**Figure 5-16: Input resistance and reactance for the 50 Ω antennas. The results for all 12 antennas are displayed.**

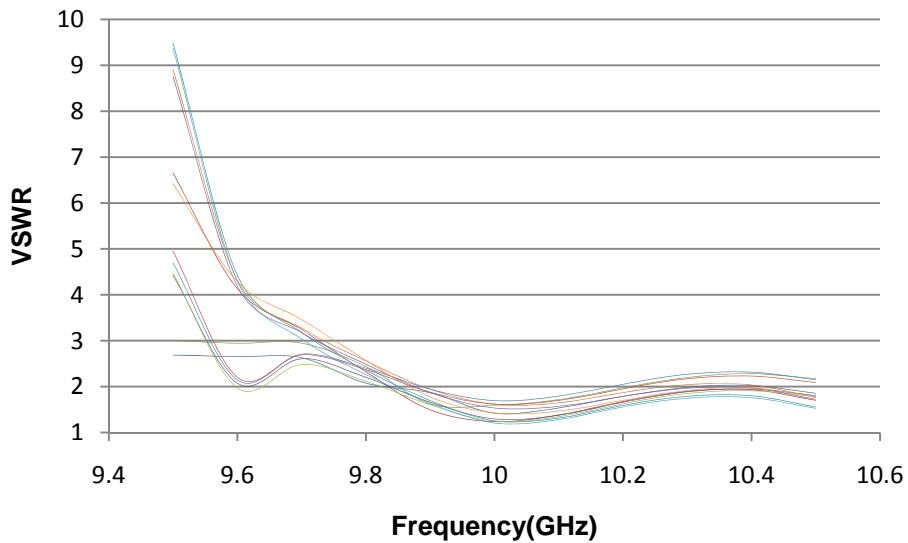


**Figure 5-17: VSWR for the 50 Ω antennas. The results for all 12 antennas are displayed.**

### 5.2.6 OUTPUT ANTENNAS - 24 Ω INPUT IMPEDANCES

The next step was to design the 24 Ω impedance antennas for the output of the power amplifier. Figure 5-18 show the input resistance of the antennas is close to 24 Ω and the reactance is close to 0 Ω. VSWR, shown in Figure 5-19, presents a bandwidth of

approximately 180 MHz. This is still appropriate for the amplifier application. Table 5-1 presents the dimensions for these antennas.

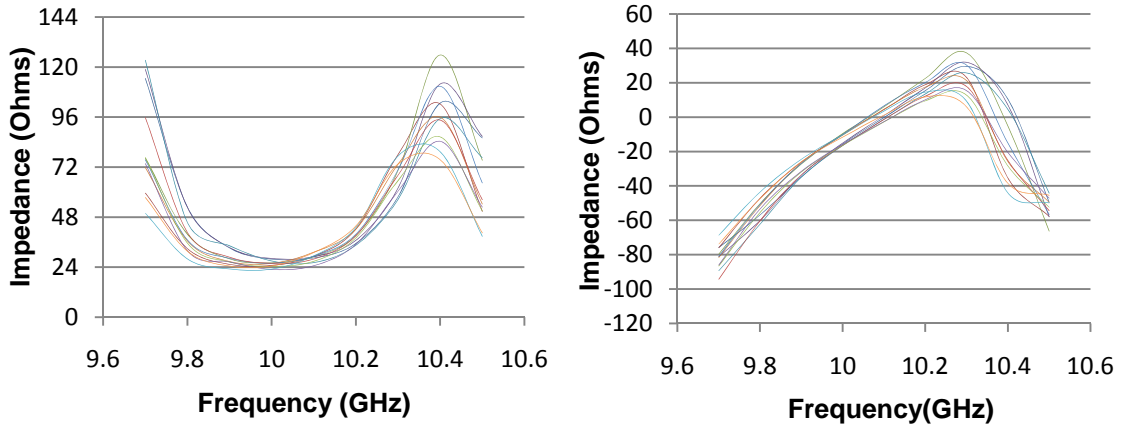


**Figure 5-18: Input reactance for the 24  $\Omega$  antennas. The results for all the 12 antennas are displayed.**

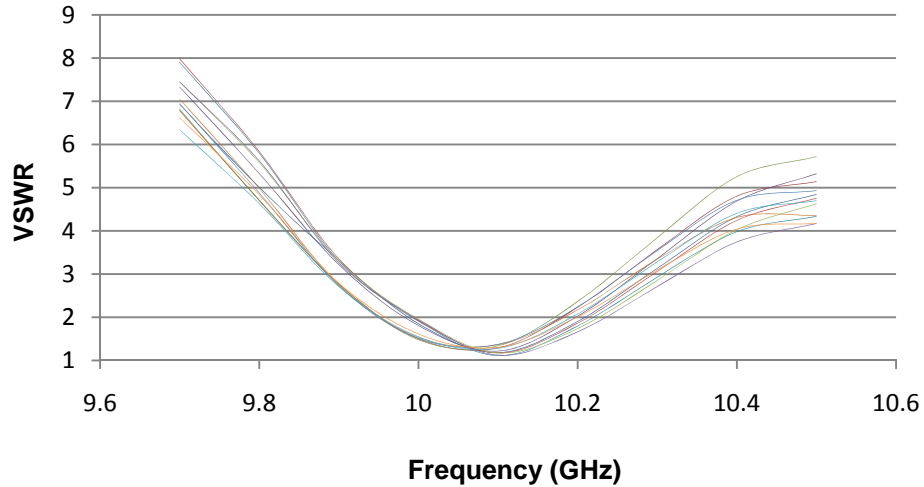


**Figure 5-19: VSWR for the 24  $\Omega$  antennas. The results for all the 12 antennas are displayed.**

### 5.2.7 50 $\Omega$ ANTENNAS WITH STUB

For the final design, a single stub was added as a termination to the second harmonic. This design was simulated with three trays. The simulated results are shown in Figure 5-20 and Figure 5-21. From these plots, it is observed that a bandwidth of 160 MHz was obtained.

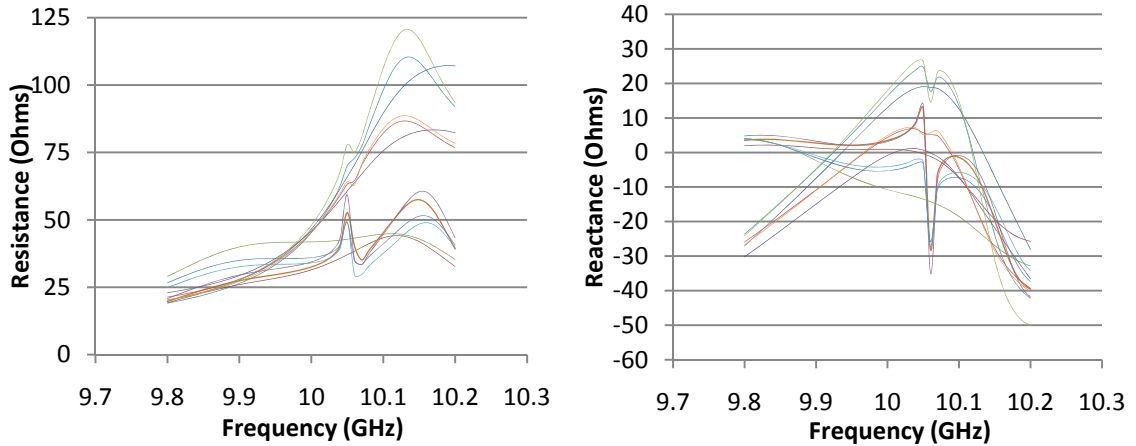


**Figure 5-20: Input resistance and reactance for the 50 Ω antennas with the stub. The results for all the 12 antennas are displayed.**

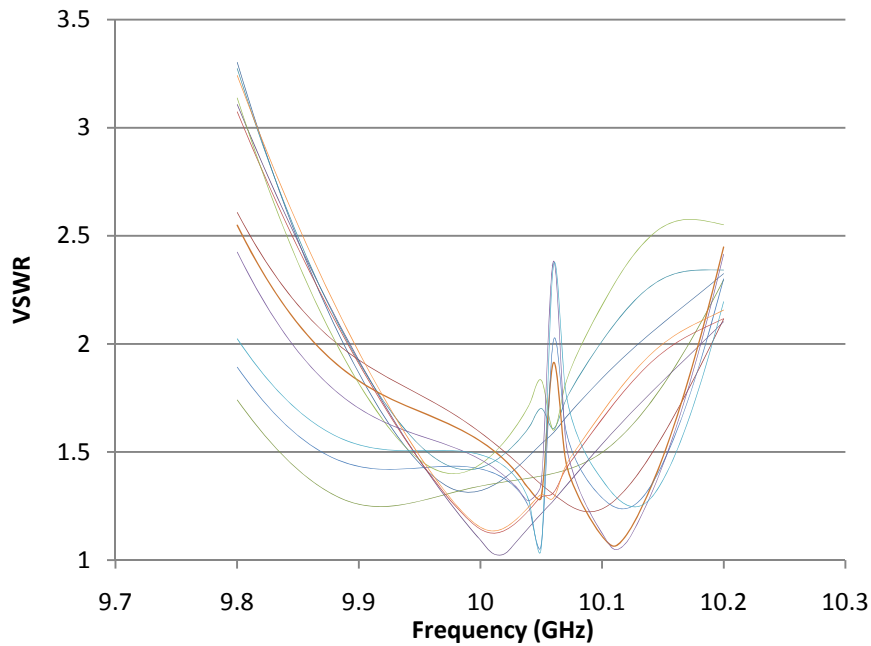


**Figure 5-21: VSWR for the 50 Ω antennas with the stub. The results for all the 12 antennas are displayed.**

Once a good result was obtained at 10 GHz, a simulation at 20GHz was done in order to prove that the stub is working at second harmonic. From this simulation, it was noted that the VSWR is greater than 3 (see Figure 5-22). However, if it is increased, in order to decrease the power losses, the bandwidth at 10 GHz is decreased because of the coupling.

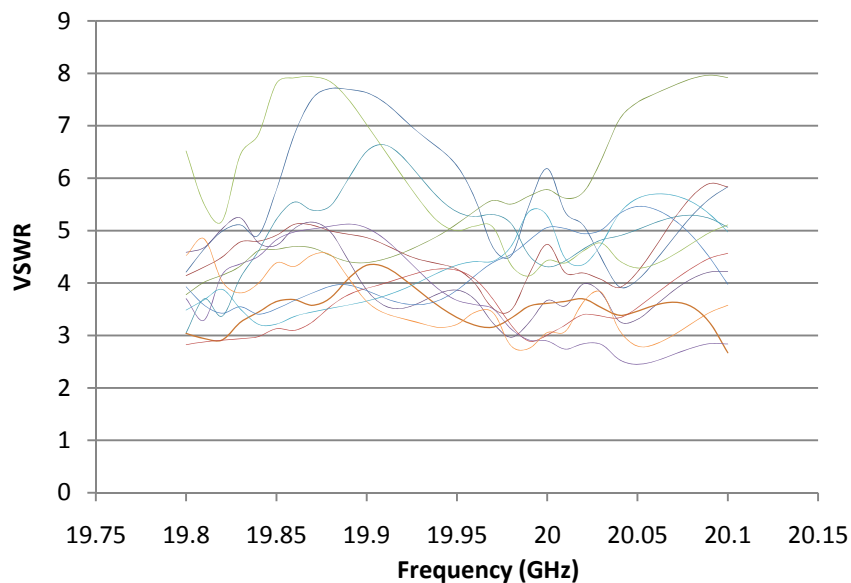


**Figure 5-22: VSWR for the 50  $\Omega$  antennas at second harmonic. The results for all the 12 antennas are displayed.**

After a 160 MHz bandwidth was achieved at 10GHz and the termination functioned at 20GHz in simulations, a setup to measure this configuration was built. Only edge antennas were measured (one for each tray) in order to facilitate the process. Two of the results are shown in Figure 5-23. Figure 5-24 shows this setup. When the simulated and measured values are compared, it can be seen that the results are very similar. The few variations are due to errors in physical construction. However, the measured results presents and excellent performance in the desired bandwidth.

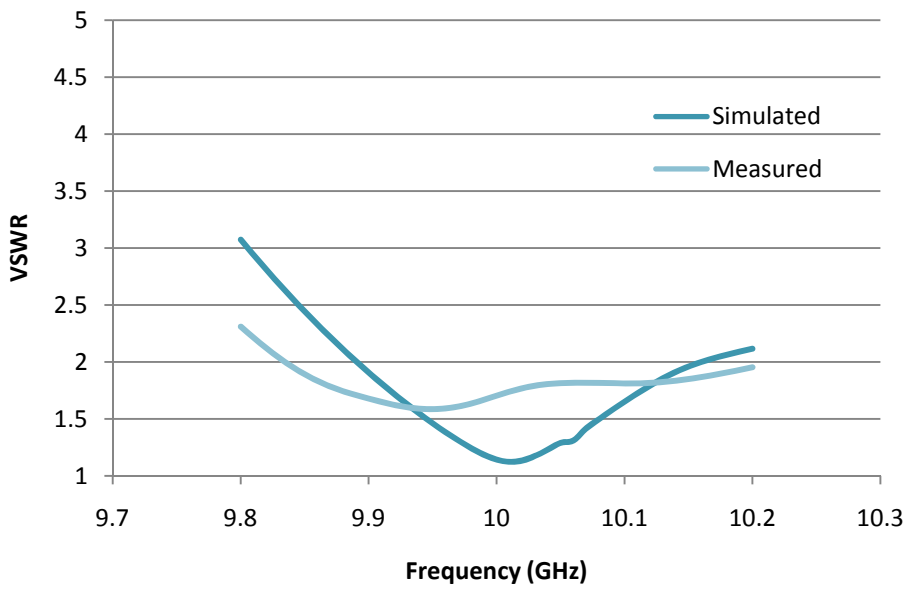
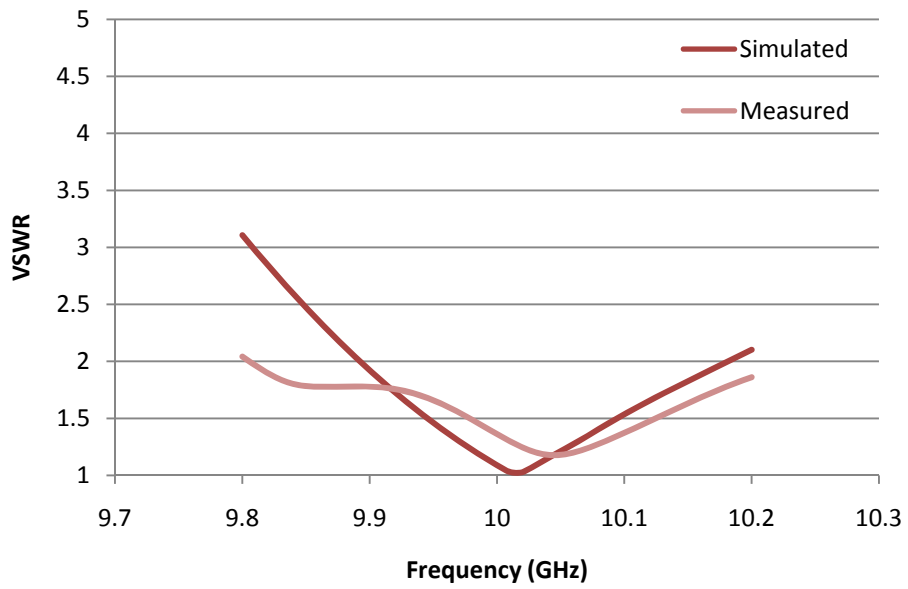


**Figure 5-23: Simulated and measured results for two antennas in the three trays configuration.**

**Table 5-1: Dimensions for the 3, 6 and 9 trays for the 65  $\Omega$  Antennas, and the 3-Trays Simulations for the 50  $\Omega$  and 24  $\Omega$  Antennas.**

		Antenna Impedances			
		24 Ohms	50 Ohms	65 Ohms	50 Ohms-Second Design
<b>Center Antennas</b>	Total Length (mm)	33	33	33	30.2
	Feed Point Position (mm)	1.7	2	1.9	2
	Feed Width (mm)	0.12	0.10	0.10	0.15
	Growth Rate, $\delta$ ( $\text{mm}^{-1}$ )	0.096	0.105	0.090	0.09
<b>Edge Antennas</b>	Total Length (mm)	33.5	34	33	32.7
	Feed Point Position (mm)	1.7	2.2	2.1	2
	Feed Width (mm)	0.08	0.06	0.1	0.1
	Growth Rate, $\delta$ ( $\text{mm}^{-1}$ )	0.096	0.103	0.91	0.9
<b>Transmission Lines</b>	Slot Width (mm)	0.0025	0.06	0.1	0.1
	separation between slots (mm)	0.395	0.28	0.2	0.5

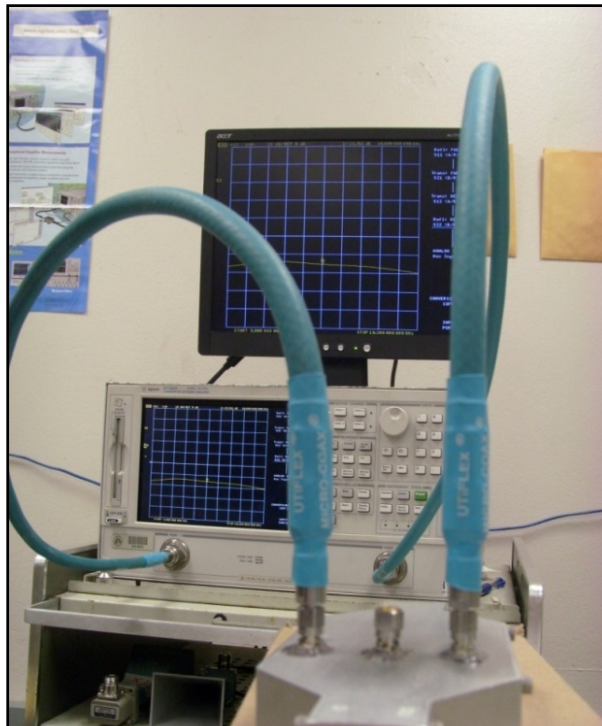


**Figure 5-24: Setup to validate the 50 Ohms antenna design.**

Given that the three tray configuration performance agreed with the simulations, the next step was to simulate and test the nine-tray configuration. In the simulations, it can be noticed that the bandwidth decreased to approximately 100 MHz. In that case, a tradeoff between bandwidth and output power has to be made in order to use this configuration. Figure 5-25 shows the simulated plots for nine trays.

Since the bandwidth is still adequate for radar applications, the antennas were built and measured. When the results are compared with simulations excellent agreements are found (see Figure 5-26).

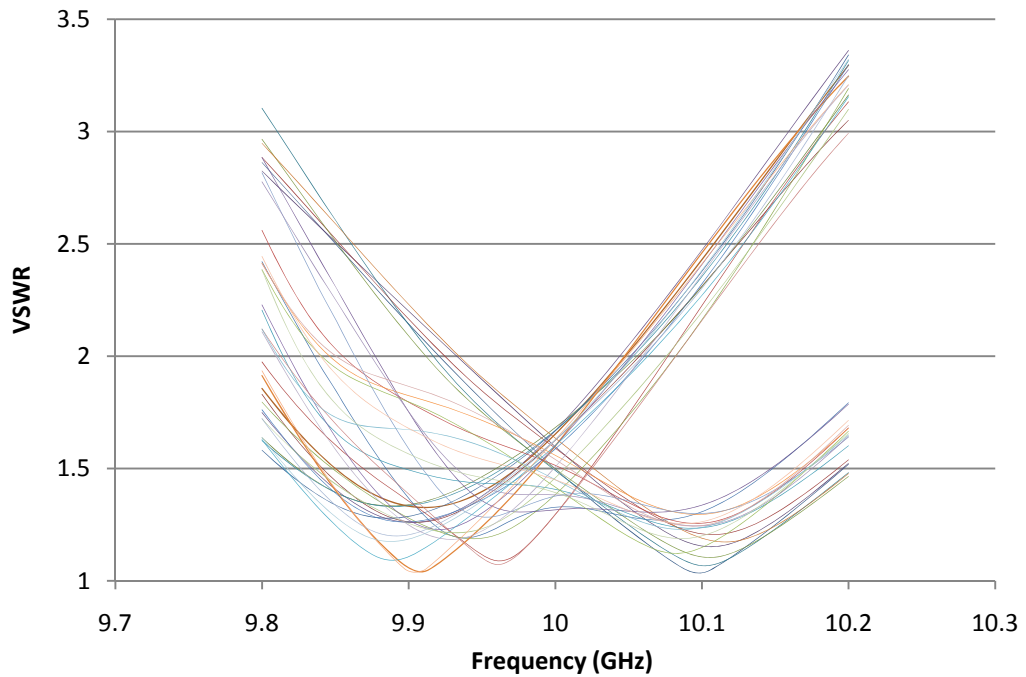


**Figure 5-25: VSWR for the 50  $\Omega$  antennas in the 9-tray configuration. The results for all the 36 antennas are displayed.**

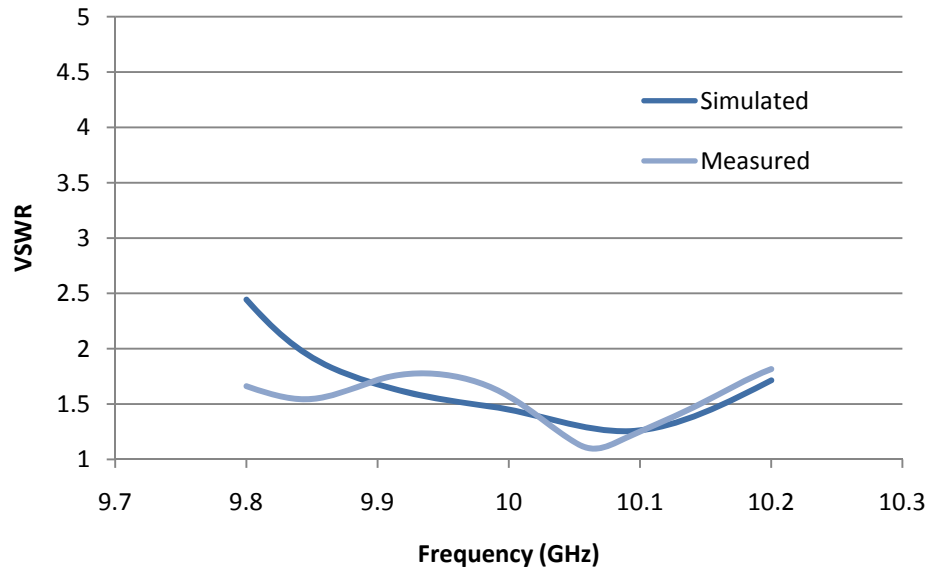
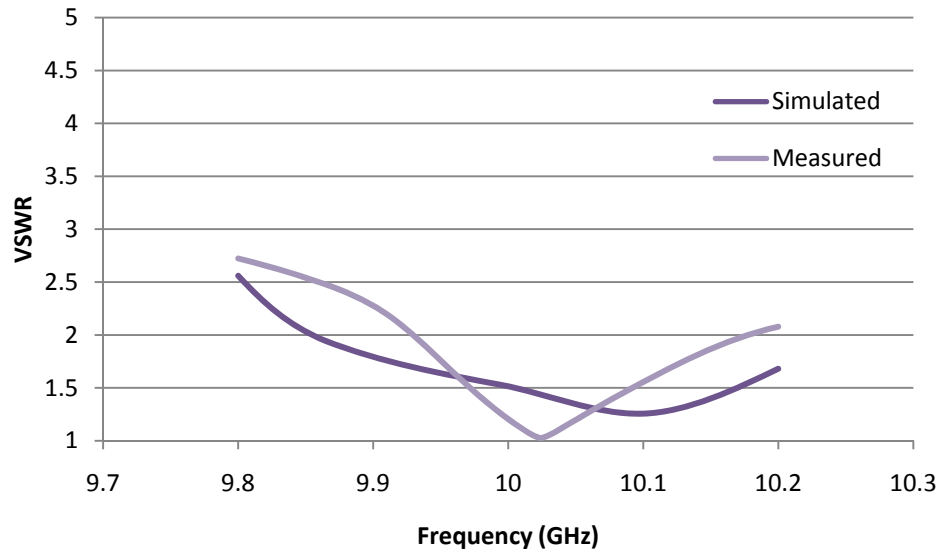


**Figure 5-26: Simulated and measured results for two antennas in the nine trays configuration.**

### 5.3 OUTPUT MATCHING DESIGN

The twelve matching networks were simulated inside the waveguide with the theoretical values. The impedance  $Z_{in}$  was equal to  $12+j14$  Ohms while the load impedance was 50 Ohms. Because of coupling, the central frequencies were shifted up (near 10.5GHz instead of 10GHz). Given that, the stubs length was adjusted to achieve a central

frequency of 10GHz in all the matching networks. The theoretical dimensions and the used values are shown in Table 5-2.

**Table 5-2: Matching network dimensions are shown. The slot width and separation of the CPW transmission line as well as lengths of the stub and transmission line are presented. All units are in mm.**

Dimension		Calculated Values (mm)	Final Values (mm)
Z <sub>o</sub>	Slot width, W	0.1	0.1
	Separation, S	0.5	0.5
Stub length, l		2.63	3.05
CPW line length, d		1.92	1.95

With those dimensions, the VSWR is maintained below 1.33 from a frequency range of 9.5 to 10.5 GHz. At 10 GHz the greatest VSWR is 1.09 (see Figure 5-27).

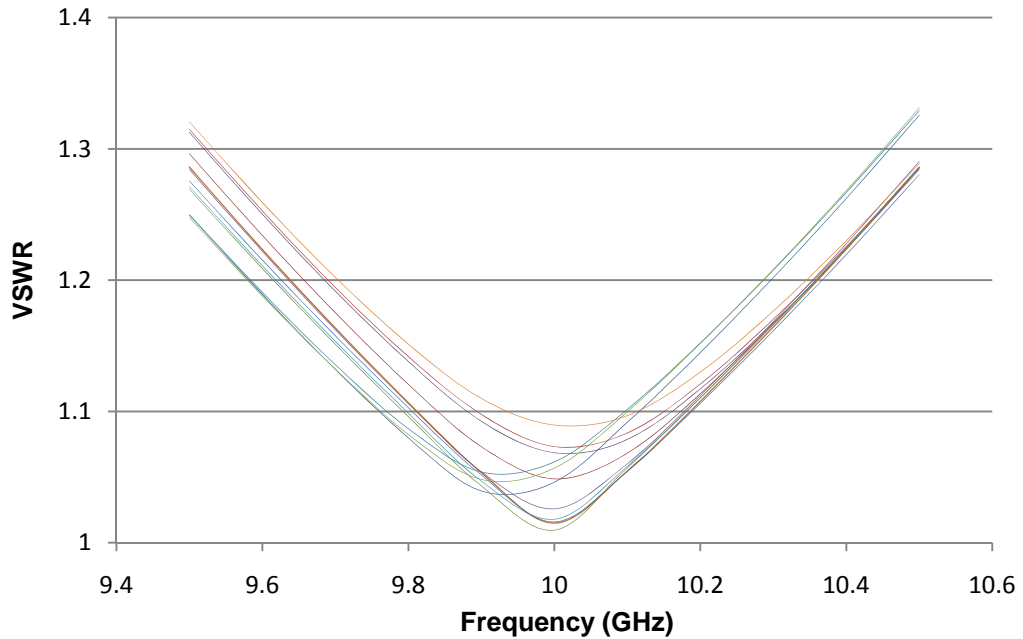


**Figure 5-27: VSWR for the match network. The results for all the 12 networks are displayed.**

# CHAPTER 6

## CONCLUSION AND FUTURE WORK

### 6.1 CONCLUSION

This thesis presented the design of a Vivaldi antenna array and proposes a spatially distributed amplifier. The design procedure for the radiating elements, the used modules and the waveguide were presented. In the case of the radiating elements, tapered slot antennas were used. Impedances of 65 Ohms were used to validate the results of 24 Ohms and 50 ohms. Finally, only 50 Ohms antennas were studied because of the difficulty to build 24 Ohms impedances antennas. The antenna arrays present a stub at the second harmonic and a 180 MHz of bandwidth.

Matching networks had to be used since the proposed amplifier needs a low impedance load. This design maintained a VSWR less than 1.1 at the frequency of interest. The bias network was done with inductors because the available space was not enough to implement an RF choke with CPW lines. The class-E module and the tray for the space distributed amplifier are shown.

### 6.2 CONTRIBUTIONS OF THIS WORK

The contributions of this work are the following:

1. Procedure and Design of Experiment analysis of a tapered slot antenna array changing dimensions in accordance with position, taking into account waveguide effects. Two papers were published:
  - a. Design of Tapered Slot Antenna Array for Space Distributed Class E Power Amplifier [27].
  - b. Design of Coplanar Waveguide Fed Tapered Slot Antenna Arrays for High-Power Space Distributed Amplifier Applications [28].

2. The design of an overmoded waveguide analyzing the transition between modes to provide low input reflection coefficient and high transmission coefficient.
3. Addition of metal sheets inside the waveguide to force three fundamentals modes.
4. Design of matching networks taking into account the effects of the waveguide.
5. Design of a class-E module with CPW lines.
6. Proposed and designed a tray for a spatially distributed amplifier using class-E modules.

### **6.3 FUTURE WORK**

The main work that remains for the continuation of this work is to implement the trays with gold instead of copper to simplify the wire bonding process. Also, the 24 Ohms impedance antennas need to be addressed in order to eliminate the matching network or decrease the start width of the 50 Ohms antennas to increase bandwidth. Additionally, the dimension  $b$  of the waveguide can be increased, without allowing other modes, to increase the antenna dimensions or to add antennas and analyze if bandwidth or power can be increased.

## REFERENCES

- [1] *Spatial Power Combining for High Power Transmitters*. Harvey, J., et al. s.l. : Microwave Magazine, IEEE, Dec 2000, Vols. I no.4, pp.48-59.
- [2] *40-W CW broad-band spatial power combiner using dense finline arrays*. Cheng, Nai-Shuo, et al. s.l. : Microwave Theory and Techniques, IEEE Transactions on, Jul 1999, Vols. 47, no.7, pp.1070-1076.
- [3] *A 60-watt X-band spatially combined solid-state amplifier*. Cheng, Nai-Shuo, et al. s.l. : Microwave Symposium Digest,1999 IEEE MTT-S International, 1999, Vols. 2, pp.539-542.
- [4] *A 120-W X-band spatially combined solid-state amplifier*. Cheng, Nai-Shuo, et al. s.l. : Microwave Theory and Techniques, IEEE Transactions on, Dec 1999, Vols. vol.47, no.12, pp.2557-2561.
- [5] *Design of waveguide finline arrays for spatial power combining*. Jia, Pengcheng, et al. s.l. : Microwave Theory and Techniques, IEEE Transactions on, Apr 2001, Vols. vol.49, no.4, pp.609-614.
- [6] *Efficiency of chip-level versus external power combining [microwave power amplifiers]*. Bryerton, E.W., Weiss, M.D. and Popovic, Z. s.l. : Microwave Theory and Techniques, IEEE Transactions on , Aug 1999, Vols. 47, no.8, pp.1482-1485.
- [7] *An efficient X-band 16-element spatial combiner of switched-mode power amplifiers*. Pajic, S. and Popovic, Z.B. s.l. : Microwave Theory and Techniques, IEEE Transactions on, July 2003, Vols. 51, no.7, pp. 1863-1870.
- [8] Cripps, Steve C. *RF Power Amplifiers for Wireless Communications*. s.l. : Artech House Inc, 2nd edition, pp. 173-199. , 2006.
- [9] *The transmission-line high-efficiency class-E amplifier*. Mader, T.B. and Popovic, Z.B. s.l. : Microwave and Guided Wave Letters, IEEE [see also IEEE Microwave and Wireless Components Letters], Sep 1995, Vols. 5, no.9, pp.290-292.
- [10] *Switched-Mode High-Efficiency Microwave Power Amplifiers in a Free-Space Power-Combiner Array*. Mader, T.B., et al. s.l. : Microwave Theory and Techniques, IEEE Transactions on, Oct 1998, Vols. 46, no.10, pp.1391-1398.

- [11] *Class-E RF Power Amplifiers*. Sokal, Nathan O. Jan/Feb 2001, Vols. pp. 9-20 .
- [12] *A broadband stripline array element*. Lewis, L., Fassett, M. and Hunt, J. s.l. : Antennas and Propagation Society International Symposium, 1974, Jun 1974. Vols. 12, no., pp. 335-337.
- [13] *Parameter study and design of wide-band wide scan dual-polarized tapered slot antenna arrays*. Chio, Tan-Huat and Schaubert, D.H. s.l. : Antennas and Propagation, IEEE Transactions on, Jun 2000, Vols. vol.48, no.6, pp.879-886,.
- [14] *Wideband Vivaldi arrays for large aperture antennas*. Chio, D. H. Schaubert and T.-H. s.l. : Proc. NFRA Conf. Perspectives on Radio Astronomy, Technologies for Large Antenna Arrays Dwingeloo, Netherlands, Sept. 1999.
- [15] Mailloux, R.C. *Phased Array Antenna Handbook*. s.l. : Second Edition. Artech House, Norwood, MA, pp. 248-251, 2005.
- [16] *A Novel MIC Slot-Line Antenna*. Prasad, S.N. and Mahapatra, S. s.l. : European Microwave Conference, 1979. 9th, pp.120-124, Oct. 1979.
- [17] *Endfire tapered slot antennas on dielectric substrates*. Schaubert, D., et al. s.l. : Antennas and Propagation, IEEE Transactions on, Dec 1985, Vols. 33, no.12, pp. 1392-1400.
- [18] *Slot Line on a Dielectric Substrate*. Cohn, S.B. s.l. : Microwave Theory and Techniques, IEEE Transactions on, Oct 1969, Vols. 17, no.10, pp. 768-778.
- [19] *Analysis of the tapered slot antenna*. Janaswamy, R. and Schaubert, D. s.l. : Antennas and Propagation, IEEE Transactions on, Sep 1987, Vols. 35, no.9, pp. 1058-1065.
- [20] *Endfire slotline antennas excited by a coplanar waveguide*. Nestic, A. s.l. : Antennas and Propagation Society International Symposium, 1991. AP-S. Digest, Jun 1991, Vols. vol.2, 24-28, pp.700-702.
- [21] *Coplanar waveguide feed linear tapered slot antenna*. Wu, X.-D. and Chang, K. s.l. : Antennas and Propagation Society International Symposium, 1993. AP-S. Digest, 28 Jun-2 Jul 1993, Vols. 1, pp.364-367 .
- [22] *Expressions for Wavelength and Impedance of a Slotline (Letters)*. Garg, R. and Gupta, K.C. s.l. : Microwave Theory and Techniques, IEEE Transactions on, Aug 1976, Vols. 24, no.8, pp. 532-532.

- [23] *Dispersion Characteristics for Wide Slotlines on Low-Permittivity Substrates (Short Paper)*. Janaswamy, R. and Schaubert, H.D. s.l. : Microwave Theory and Techniques, IEEE Transactions on , Aug 1985, Vols. 33, no.8, pp. 723-726.
- [24] *Characteristic Impedance of a Wide Slotline on Low-Permittivity Substrates (Short Paper)*. Janaswamy, R. and Schaubert, D.H. s.l. : Microwave Theory and Techniques, IEEE Transactions on, Aug 1986, Vols. 34, no.8, pp. 900-902.
- [25] *The square kilometer array (SKA) antenna*. Schaubert, D.H., et al. s.l. : Phased Array Systems and Technology, 2003. IEEE International Symposium on, pp. 351-358, 14-17 Oct. 2003.
- [26] *Experimental results of 144-element dual-polarized endfire tapered-slot phased arrays*. Holter, H., Chio, Tan-Huat and Schaubert, D.H. s.l. : Antennas and Propagation, IEEE Transactions on, Nov 2000, Vols. 48, no.11, pp.1707-1718.
- [27] *Design of Tapered Slot Antenna Array for Space Distributed Class E Power Amplifier*. Rivera, A., Rodriguez, R., Accepted 2009 IEEE AP-S International Symposium on Antennas and Propagation, June 01-05, 2009.
- [28] *Design of Coplanar Waveguide Fed Tapered Slot Antenna Arrays for High-Power Space Distributed Amplifier Applications*. Rivera, A., Rodriguez, R., Antennas Applications Symposium, pp.233-249, 15-18 Sept. 2008